RIS-Assisted Proactive Handover in mmWave Networks

Journal:	*IEEE Transactions on Vehicular Technology*
Manuscript ID	VT-2025-03912
Manuscript Type:	Regular Paper
Date Submitted by the Author:	10-Jul-2025
Complete List of Authors:	Adnan, Alaa; University of Glasgow James Watt School of Engineering Al-Quraan, Mohammad; University of Glasgow James Watt School of Engineering Zoha, Ahmed ; University of Glasgow James Watt School of Engineering Butt, M. Majid; Nokia Solutions and Networks Holdings USA Inc Irving Muhaidat, Sami; Khalifa University Department of Electrical Engineering and Computer Science; Carleton University Department of Systems and Computer Engineering Imran, Muhammad Ali; University of Glasgow James Watt School of Engineering Di Renzo, Marco; Universite Paris-Saclay CentraleSupelec; King's College London Department of Informatics Mohjazi , Lina ; University of Glasgow James Watt School of Engineering
Keywords:	Intelligent networks, Millimeter wave communication, MIMO systems, Reconfigurable antennas, Reconfigurable architectures

RIS-Assisted Proactive Handover in mmWave Networks

Alaa Adnan, *Graduate Student Member, IEEE,* Mohammad Al-Quraan, *Graduate Student Member, IEEE,* Ahmed Zoha, *Senior Member, IEEE,* M. Majid Butt, *Senior Member, IEEE,* Sami Muhaidat, *Senior Member, IEEE,* Muhammad Ali Imran, *Fellow, IEEE,* Marco Di Renzo, *Fellow, IEEE,* and Lina Mohjazi, *Senior Member, IEEE*

***Abstract*—Millimeter-wave (mmWave) networks are highly vulnerable to line-of-sight (LoS) blockages. Vision-aided wireless communications (VAWC) enable proactive handovers (PHO) to address blockages in advance, ensuring seamless connectivity. However, PHO becomes challenging in scenarios where a nearby base station (BS) is unavailable. In such cases, reconfigurable intelligent surfaces (RIS) can restore connectivity. For RIS-assisted mmWave links to be practically deployed for a PHO, the RIS configuration time must be considered to ensure timely PHO. This key challenge stems from the large number of RIS elements, which limits the deployment in time-sensitive applications. For practical deployment, the RIS-assisted link must achieve a trade-off between 1) reducing signal processing complexity and 2) maintaining link quality. This can be accomplished by optimizing the RIS-assisted PHO process through minimizing the number of RIS elements required to maintain connectivity and accounting for the handover timing constraints. This work proposes a novel RIS-assisted PHO approach to maintain seamless connectivity during a blockage event. We formulate an optimization problem using particle swarm optimization (PSO) to determine the optimal end-to-end RIS-assisted link configuration setup. The proposed PSO approach reduced the required number of RIS elements to establish a link by 15% without compromising the desired link rate improving the signal strength by 15 to 30 dBm in the blocked area. Moreover, RIS configuration time is integrated into the PHO framework, ensuring accurate timing.**

***Index Terms*—Reconfigurable Intelligent Surfaces, Multiple Input Multiple Output,Vision Aided Wireless Communications, Particles Swarm Optimization.**

I. INTRODUCTION

Millimeter-wave (mmWave) technology has emerged as a promising candidate for sixth-generation (6G) networks due to its ability to support higher transmission rates [1]. Beamforming is envisioned to play a key role in mmWave systems, providing spatial reuse and reducing interference [2]. However, in terms of reliability, beamforming-based mmWave connectivity mainly relies on directive line-of-sight (LoS) links due to channel sparsity, which limits the usefulness of multipath components [3]. This makes mmWave signals highly susceptible to blockages, causing severe signal degradation when a LoS beam is obstructed.

Vision-aided wireless communication (VAWC) frameworks are expected to play a crucial role in 6G networks by leveraging visual information of the wireless environment to enable key applications including optimal beam selection based on user location [4], throughput estimation for choosing the best base station (BS) to serve a user [5], and, most importantly, beam blockage prediction in mmWave networks [6]. Meanwhile, reconfigurable intelligent surfaces (RIS) have emerged as a promising technology for enhancing signal quality and mitigating LoS blockages as the RIS can steer the signal towards a desired location using RIS-assisted links [7].

In our previous work [8], we integrated these two concepts into a unified framework to enhance reliability and address the blockage issue. The findings revealed that to provide acceptable signal strength, the RIS-assisted link must utilize a large RIS array to improve the signal quality. The need for larger RISs is attributed to the nearly passive nature of the RIS and the fact that the effective aperture area of an RIS is typically smaller than its actual physical area, further increasing the demand for a larger RIS to enhance link performance. The work in [9] introduced a mathematical model that accounts for the aperture area efficiency and proposed a modified path loss model based on the effective RIS area. Notably, the model considered the far-field assumption and estimated the RIS diameter to be approximately 20mm for a frequency of 28GHz, with an even smaller effective RIS area available for establishing a link. As a result, at higher frequency bands, the RIS effective area becomes even smaller. To overcome this limitation, achieving better performance requires deploying physically larger RISs.

The need for physically larger RISs operating in the mmWave band necessitates denser RIS configurations composed of smaller elements, due to the shorter wavelengths at these frequencies. Since each RIS element typically has an area smaller or equal to half of a wavelength squared, this implies that a significant number of elements can be accommodated per unit area. For instance, the authors in [10] fabricated and tested an RIS in both near-field and far-field scenarios. The fabricated RIS had an area of $10\text{ cm} \times 10\text{ cm}$, operated at 28GHz, and contained 400 RIS elements within this relatively small space. Deploying dense RISs operating in the mmWave

A. Adnan, M. Al-Quraan, A. Zoha, M. A. Imran and L. Mohjazi, are with the James Watt School of Engineering, University of Glasgow, Glasgow, G12 8QQ, UK. (e-mails: A.Bibi.1@research.gla.ac.uk, {Mohammad.Alquraan, Ahmed.Zoha, Muhammad.Imran, Lina.Mohjazi}@glasgow.ac.uk).

M. Majid Butt is with with Nokia Standards, USA. (e-mail: Majid.Butt@nokia.com).

S. Muhaidat is with the KU 6G Research Center, Department of Computer and Communication Engineering, Khalifa University, Abu Dhabi 127788, UAE, and also with the Department of Systems and Computer Engineering, Carleton University, Ottawa, ON K1S 5B6, Canada. (e-mail: sami.muhaidat@ku.ac.ae).

M. Di Renzo is with Université Paris-Saclay, CNRS, CentraleSupélec, Laboratoire des Signaux et Systèmes, 3 Rue Joliot-Curie, 91192 Gif-sur-Yvette, France (e-mail:marco.di-renzo@universite-paris-saclay.fr), and with King's College London, Centre for Telecommunications Research Department of Engineering, WC2R 2LS London, UK. (e-mail:marco.di_renzo@kcl.ac.uk).

band introduces several challenges, such as complex channel modeling, extensive channel estimation, and complex beam training, limiting the RIS application in real-time or time-sensitive applications.

The complexity of channel modeling arises from the fact that dense RISs necessitate near-field channel modeling. Assuming a fixed inter-element spacing equal to half a wavelength, the physical size of the RIS which determines the Fresnel distance is directly tied to the number of elements. With such a large number of RIS elements, satisfying far-field conditions often requires distances that exceed the Fraunhofer distance. This condition may result in a scenario where the link between the BS and the RIS operates in the far-field region, while the link between the RIS and the user remains in the near-field region [11].

Channel estimation in mmWave systems leveraging a large RIS with a high number of RIS elements presents a significant challenge. For instance, the study in [12] introduced an algorithm for channel estimation in near-field large-scale MIMO arrays, where the algorithm's complexity for non-line-of-sight (NLoS) paths depended on the number of scatterers required to reconstruct the signal. In the context of RIS channel estimation, near-field complexity is directly influenced by the number of RIS elements. In the next section, we will present the related work for beam blockage management in mmWave networks as an alternative to the explicit channel estimation approach and highlight the effect of the increased number of RIS elements on the system performance.

A. Related Work

In this section, we present state-of-the-art research that proposes solutions to beam blockages in high-frequency bands. The reviewed studies focus on beam blockage prediction and beam blockage mitigation by RIS-assisted links as an alternative to a blocked LoS.

1) Beam Blockage Prediction: Beam blockage prediction plays a crucial role in ensuring reliable communication, as it triggers the handover process to a link with better conditions than the blocked one. Two primary approaches are considered for predicting blockages: wireless information-based approaches and sensing information-based approaches [13]. Our focus will be on the sensing-based approach since it is the approach we are proposing in this work.

For sensing-based approach, various data acquisition techniques are employed for link blockage prediction, including VAWC frameworks, light detection and ranging (LiDAR) sensing, and radar-based blockage prediction. For instance, the work in [14] leveraged a VAWC framework, using a set of RGB images with predefined beamforming vectors to train a deep learning (DL) model for blockage prediction in mmWave networks. The work in [15] proposed the use of RGB images with depth cameras to train a machine learning (ML) model called adaptive regulation of wave vectors (AROW), facilitating proactive BS selection in blockage scenarios. The selection criterion was based on throughput estimations to ensure the best link for a handover. Additionally, [16] utilized LiDAR to acquire point cloud data for mmWave link quality prediction, forecasting radio propagation fluctuations caused by pedestrian obstructions. The work in [17] demonstrated that integrating radar-based sensing with mmWave BSs provides valuable information, such as velocity and range, which can aid in predicting network obstacles.

2) Beam Blockage Mitigation by RIS-Assisted Links: RIS-assisted links provide an effective solution for replacing blocked LoS links by redirecting incident signals to obstructed users. The potential to reduce channel estimation and beam training overhead has garnered significant interest in enhancing the practical deployment of RISs, particularly for time-critical or real-time applications.

The study in [18] aimed to optimize RIS performance by jointly designing BS beamforming and RIS reflection coefficients. The proposed approach maximized the user's sum rate by directly optimizing received pilots at the BS using a graphical neural network (GNN) learning model. This method eliminated the need for explicit channel estimation. Results demonstrated that incorporating additional information, such as user location reduced pilot transmission achieving optimal beamforming and RIS reflection settings. Despite these improvements, the complexity of the beamforming matrix design remains directly proportional to the number of RIS elements, leading to increased training delays. This led the authors to assume that GNN training is performed offline to mitigate the impact of runtime delays in online scenarios.

Another promising approach involves intelligent RIS beam management (BM) and beam training (BT) instead of explicitly estimating channel state information (CSI). For example, [19] trained a ML model within a BM framework to process environmental and user mobility data, enhancing BM in beam blockage scenarios. The work in [20] employed BT to estimate the best beam selection for the receiver. However, this method heavily depended on RIS phase shifter resolution, often assuming an ideal continuous phase shifter capable of selecting the optimal beam with minimal directivity loss.

Furthermore, [21] proposed a joint active and passive beamforming design for optimal beam selection in RIS-assisted networks, utilizing the concept of a channel knowledge map (CKM). This approach builds a site database that correlates beams with users' geographical locations, aiding in optimized beam selection. Also, this work highlighted the fact that BT overhead is directly related to the number of RIS elements, and with the large number of mmWave RIS elements, BT will be a challenging task.

Despite advancements in beam blockage prediction and mitigation techniques, integrating an RIS with a VAWC framework for a seamless RIS-assisted handover has not been explored in prior studies as the authors assumed the availability of a BS to which the blocked user can be handed over. However, in some scenarios, a second BS may not be available. Additionally, most RIS-related works assume that user locations and blockage information are either known at the BS or rely on probabilistic models, which are unsuitable for dynamic real-time scenarios. Another overlooked factor is the impact of RIS configuration time on system performance.

Moreover, even with BM and BT techniques, mmWave RIS implementations still require a large number of RIS elements

for acceptable performance. In our previous study [8] we performed a system performance analysis for a mmWave RIS-assisted link operating at 60GHz, the findings indicated that at least 1000 RIS elements are necessary to establish a link with sufficient signal strength, making signal processing a highly complex task and increasing BT overhead. Therefore, optimizing the RIS-assisted handover process by minimizing the required number of RIS elements while maintaining link quality is crucial for practical deployment.

B. Motivation and contribution

The aforementioned research studies indicate that realizing RIS-assisted mmWave communication requires a significantly large number of RIS elements. This work aims to leverage an RIS-assisted link in a proactive handover (PHO) process to replace a blocked LoS connection. However, deploying large-scale mmWave RIS-assisted communication systems presents several challenges, which become critical bottlenecks for time-sensitive applications such as PHO, as they are constrained by narrow time windows for triggering the handover process.

To effectively leverage RIS for PHO, two key deployment challenges must be addressed:

- Ensure that the RIS has a sufficient number of elements to maintain the required link quality.
- Ensure that the time needed to configure the phase shifts of the RIS elements is within the acceptable time limit to trigger handover before the occurrence of a blocking event.

From a practical deployment perspective, finding a trade-off between achieving the desired RIS-assisted link quality and mitigating signal processing complexity, particularly in channel estimation and modeling, is crucial. This trade-off can be realized by efficiently minimizing the number of RIS elements while maintaining acceptable link quality, such as a target achievable rate. Such an approach not only reduces the complexity of channel estimation and BT overhead but also enhances the feasibility of RIS-assisted links for real-time applications. Since PHO depends on accurate timing to trigger the process, the time required for RIS configuration becomes a critical factor in ensuring a successful PHO. However, no studies have specifically focused on the impact of RIS configuration time on PHO timing. In the surveyed literature, RIS configuration time was either estimated or assumed for purposes unrelated to PHO considerations.

The work presented in [22] suggested that RIS configuration response times need to fall within a granular range of 20 to 100 milliseconds (ms) to support effective communications. The study in [23] employed the STM32L071V8T6 microcontroller unit to control RIS phase shift configurations, reporting a configuration time of less than 35 ms. Meanwhile, the work in [10] utilized a field-programmable gate array (FPGA) for RIS phase shift control, where the configuration delay ranged from 0.22 ms to 7 ms, depending on the number of RIS elements. These measurements also used to indicate wiring complexity in RIS fabrication, highlighting the challenges of managing more mmWave RIS elements, including greater fabrication difficulty, control complexity, and longer configuration time.

In these studies, the RIS configuration time was not considered within the context of a communication framework such as PHO. A deeper understanding of the factors influencing RIS configuration time is essential for the effective and practical deployment of RIS-assisted links in time-critical operations such as handovers and user tracking. To the best of the authors' knowledge, no prior work has addressed the impact of RIS configuration time on PHO in RIS-assisted links.

mmWave RIS-assisted systems are envisioned to play a significant role in 6G networks, enabling the realization of smart environments (SE) supporting applications such as road safety and autonomous vehicles in ultra dense networks (UDNs) all of which demand seamless and uninterrupted connectivity. However, considering the challenges outlined above, deploying RISs with a large number of elements introduces several issues that hinder the practical implementation of RIS-assisted links. Therefore, achieving a balance between RIS link quality and minimizing the RIS configuration time in which both are directly related to the number of RIS elements is crucial for enabling timely handover execution. Since the primary objective of this work is the effective deployment of RIS-assisted links to replace blocked mmWave LoS connection within a PHO framework, addressing these challenges is essential. In this context, the key contributions of this work can be summarized as follows:

- Integration of RIS-assisted mmWave connectivity within a novel VAWC framework to enable blockage prediction and precise user localization, thereby facilitating accurate beam steering from the RIS toward the blocked region.
- Proposing a novel RIS-assisted PHO framework that explicitly incorporates RIS configuration time into the PHO timing process, ensuring accurate triggering during LoS blockage scenarios.
- An optimization algorithm is proposed to enhance the responsiveness of the RIS-assisted PHO process by minimizing RIS configuration time, while maintaining the desired link quality.

The rest of this paper is organized as follows: In Section II, the system and channel models are presented. Section III discusses the problem formulation and optimization approach. Section IV introduces the proposed RIS-assited PHO framework. Section V provides the results and key findings. Finally, Section VI gives concluding remarks.

II. System and channel models

In this section, we provide a comprehensive description of the RIS architecture and configuration time estimation, which will be integrated into the VAWC PHO framework, along with the system and channel models.

A. RIS Configuration Time Estimation

In order to effectively deploy an RIS-assisted link in a PHO procedure, the RIS configuration time required to steer the signal toward a blocked area must be accounted for to ensure accurate triggering and seamless connectivity.

This work builds upon our previous study [8], which proposed a PHO framework (see Fig. 1) that leverages RIS-assisted beamforming in a blockage scenario (see Fig. 2). The RIS-assisted beam is selected from a pre-stored set of RIS beamforming configurations maintained in a CKM database. However, the PHO framework in [8] did not account for RIS configuration time as part of the PHO timing scheme, which is a critical factor for ensuring accurate PHO execution.

The framework proposed in [8] was based on the original PHO framework introduced in [6], which utilized VAWC and RGB cameras powered by the You Only Look Once version 3 (YOLOv3) object detection algorithm to detect blockages. The detected blockage data was then used to train a neural network (NN), which relied on user mobility speed to determine the optimal triggering point for the PHO process. However, the framework in [6] did not consider PHOs involving an RIS. Instead, it proposed performing a PHO to a secondary BS when a blockage occurs. In practice, a secondary BS may not always be available as explained in section I, making an RIS-assisted link a promising and practical alternative for handover and, thus, worth further investigation.

In the original framework proposed by [6], two important timing factors were estimated: the execution time T_{exec} and the waiting time T_{W} before triggering the handover. T_{exec} is defined as the time required for the proposed algorithm to be completed, starting when the images are captured by the BS and processed for blockage detection until the PHO process is completed. The value of T_{W} is given as follows [6]

$$T_W = T_{\text{to-BLK}} - T_{\text{exec}} \ , \tag{1}$$

where $T_{\text{to-BLK}}$ represents the time for a user to encounter a blockage. T_W varies based on the user's location and movement speed. Selecting the value of T_W is critical for defining the optimal PHO trigger region, allowing the algorithm to determine the best time to perform the PHO.

In order to integrate the RIS as part of the PHO framework T_{exec} must include T_c the RIS response time represented by the required configuration time to steer the signal to a blocked user. As a result, the updated execution time, denoted as $T_{\text{exec}}^{\text{RIS}}$, can be expressed as

$$T_{\text{exec}}^{\text{RIS}} = T_{\text{exec}} + T_{\text{c}} \ , \tag{2}$$

This leads to a new waiting time, $T_{\text{W}}^{\text{RIS}}$, which is given by

$$T_{\text{W}}^{\text{RIS}} = T_{\text{to-BLK}} - T_{\text{exec}}^{\text{RIS}} \ , \tag{3}$$

The new $T_{\text{W}}^{\text{RIS}}$ now includes the RIS configuration time T_c, in order to be able to estimate T_c we examine the RIS architecture and identify the factors contributing to the configuration time.

The design approach for RIS can vary based on multiple factors, such as indoor or outdoor deployment, operating frequency, RIS element design, and several other considerations. This work does not focus on the specific details of the radio frequency design aspects of RIS. Instead, it emphasizes the control layer setup and its impact on the configuration time.

The RIS consists of three main layers, as shown in Fig. 3: the front layer, which is a grid of RIS elements; the RIS back-layer board; and the control layer. The front layer of the RIS board typically consists of N RIS elements, each embedded with B diodes to control the phase shift of the incident signal for beam steering. The most commonly deployed diodes include varactor diodes [24] and PIN diodes [25].

The control layer is responsible for transmitting configuration bits to the RIS back-layer board. The back layer of the RIS board houses a set of logic circuits that control the diodes embedded in each RIS element, enabling them to switch on or off as needed [26]. This layer typically contains multiple shift registers, where the number of registers is generally $\leq N$, depending on the number of diodes embedded in each element and the shift register bus capacity. Since each diode requires one bit to be switched on or off, the shift registers are used by the controller layer to push the configuration bits via serial-to-parallel transmission, efficiently controlling the diode states. Different setups of shift registers controlling the RIS elements are presented in [10], [25], and [27].

The configuration time required for the RIS depends on several factors, including the transmission rate of the control board, the clocking rate of the shift registers, the number of RIS elements, and the number of diodes embedded within each element [10]. Thus, the codeword, representing the total number of bits required to configure the RIS, is determined by multiplying the total number of RIS elements by the number of diodes in each element. Each bit is used to switch a single diode on or off, enabling the desired beamforming setup of the RIS. When configuring the RIS remotely from the server, the interface speed directly impacts the configuration time. However, if the configuration states are stored locally in the microcontroller layer and the required codeword is directly pushed to the shift registers, the configuration time depends primarily on the clocking rate of the shift registers [10]. The work in this paper adopts the latter concept, and accordingly, the required time for RIS configuration is expressed as

$$T_c = \frac{NB}{C_{lk}} \ , \tag{4}$$

where C_{lk} represents the clocking rate of the shift registers.

From equation (4), along with the additional delays accounted for in equation (3), it can be deduced that reducing signal processing complexity and BT overhead while ensuring a faster RIS configuration response requires minimizing N without compromising link quality. By identifying the optimal value of N, we can estimate the RIS configuration time. As described in equation (4), N is a key factor in estimating T_c, since both B and Clk are fixed for each element and the shift register. This optimization approach will be further explored in Section III, where the proposed algorithm to achieve this goal will be introduced.

B. System Model

We consider a BS operating in the mmWave band, assisted by an RIS, where the BS transmits to a single-antenna user. The BS coverage area is served by multiple uniform linear array (ULA) sectors, with each ULA responsible for a specific segment of the coverage area. Each ULA sector comprises M antenna elements. To monitor the environment, the BS

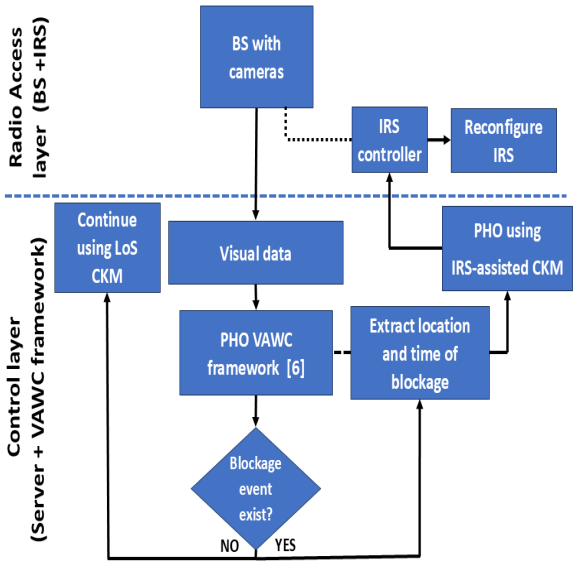

Figure 1: RIS-assisted PHO framework [8].

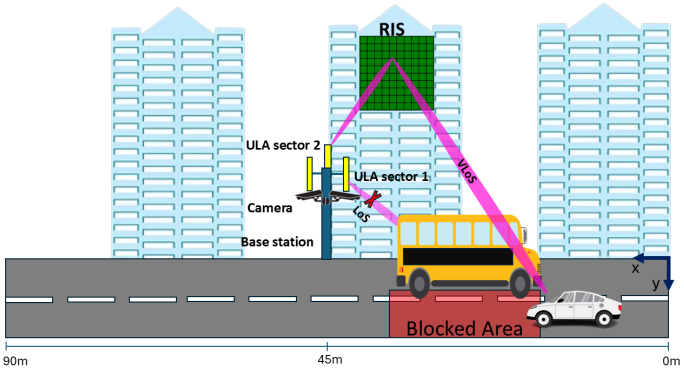

Figure 2: RIS-assisted vision-aided BS setup.

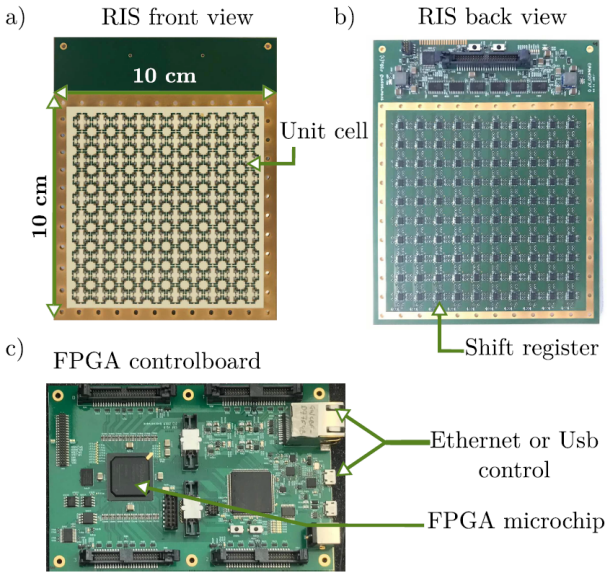

Figure 3: RIS controller board: (a) front layer of RIS elements grid, (b) back layer of shift registers grid, and (c) RIS controller board [10].

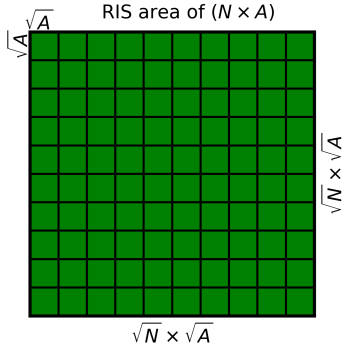

Figure 4: RIS area equals to $N \times A$.

is equipped with a set of cameras that oversee the street, as illustrated in Fig. 2. These cameras are used to determine the user's location and detect potential blockages [28].

The system employs orthogonal frequency-division multiplexing (OFDM) with K subcarriers as the resource allocation scheme for radio access. The mmWave BS system utilizes an analog beamforming technique, where the user is served by a beam represented by a beamforming vector selected from a predefined codebook $\mathcal{F} = \{f_i\}_{i=1}^{B_m}$, where $\mathbf{f}_i \in \mathbb{C}^{M\times 1}$ and B_m represents the total number of beams. Each beam, denoted as $\mathbf{f}_i$, can be expressed as follows

$$\mathbf{f}_i = \frac{1}{\sqrt{M}} \begin{bmatrix} 1 & e^{j2\pi \frac{d}{\lambda} \sin\theta_i} & \dots & e^{j2\pi \frac{d}{\lambda}(M-1)\sin\theta_i} \end{bmatrix}^T, \quad (5)$$

where $j = \sqrt{-1}$, T represents the transpose operation of a vector, d is the antenna element spacing, λ is the wavelength of the transmitter, and $\theta_i \in \left\{ \frac{2\pi i}{B_m} \right\}_{i=0}^{B_m-1}$ denotes the steering angle from the BS towards the desired user.

This study adopts the blockage scenario from the original dataset [29], where co-located cameras detect a bus obstructing the LoS signal to the served user. We extend the system setup by introducing an RIS, as illustrated in Fig. 2, to address anticipated beam blockages within the VAWC framework proposed in [6]. Instead of performing a handover to a secondary BS, as suggested in [6], this work proposes establishing a virtual line-of-sight (VLoS) link using the RIS. This VLoS link is leveraged by the PHO procedure as an alternative to the obstructed LoS link.

The RIS is comprised of elements, each of an area given by $A = \left(\frac{\lambda}{2}\right)^2$. The dimensions of each element are $(\sqrt{A} \times \sqrt{A})$, the elements are arranged in a planar square grid of size $(\sqrt{N} \times \sqrt{A})$. The total area of the RIS is $(N \times A)$ [30] as illustrated in Fig. 4. We assume the RIS is mounted on the facade of a building located behind the BS at a sufficient height to overcome obstructions. The RIS can dynamically steer the beam using a predefined $N \times N$ codebook, denoted by $\mathcal{V}$, comprised of steering coefficients expressed as

$$v_{mn} = \alpha e^{j\frac{2\pi d_{\text{RIS}}}{\lambda}\sin\theta_{mn}}, \quad (6)$$

where $v_{mn} \in \mathbb{C}^{N\times N}$, α is the reflection coefficient of each RIS element, and $m, n = 1, \dots, N$. Additionally, d_{RIS}

represents the RIS element spacing, and $\theta_{mn} \in [0, 2\pi]$ denotes the RIS steering angle.

To facilitate the PHO, each ULA sector is equipped with a camera to capture visual information. This data is processed by the VAWC framework to extract critical parameters for predicting a blockage event in advance, such as the existence of a blocking object, the user's speed toward the blocked area, and the estimated time and location of the blockage. Based on this information, the VAWC framework enables the BS to steer the RIS beam toward the anticipated blockage area, leveraging the PHO framework illustrated in Fig. 1 to define the optimal time for triggering the PHO.

C. LoS Channel Model

The user transmits a pilot signal, which is used to train the beam set B_m and select the optimal beam that maximizes the signal-to-noise ratio (SNR). This work adopts the pilot signal/beam training methodology described in [13]. Once the optimal beam is identified, it is utilized for downlink communication. The baseband mmWave signal transmitted from the BS to the user over a LoS link, in the absence of a blockage, is expressed as

$$y_{\text{los},k} = \mathbf{G}_{\text{los},k}\mathbf{f}^{\star}_{\text{los},k}s_{\text{los},k} + n_{\text{los},k} \ , \tag{7}$$

where, $s_{\text{los},k}$ represents a transmitted symbol, $n_{\text{los},k} \sim \mathcal{CN}(0, \sigma^2)$ represents the additive white gaussian noise (AWGN) for the k-th subcarrier with zero mean and variance of σ^2, $\mathbf{G}_{\text{los},k}$ is the channel gain which is expressed as [6]

$$\mathbf{G}_{\text{los},k} = \sqrt{\beta_k}\,(\mathbf{h}_k)^T e^{\left(j2\pi\frac{kd}{K\lambda}\right)} f(\theta,\phi)_k \ , \tag{8}$$

In equation (8), β_k represents the large-scale fading coefficient, $f(\theta,\phi)_k$ is the function of the angles of departure and arrival, respectively, where θ is the azimuth angle and ϕ is the elevation angle. $h_k \in \mathbb{C}^{M\times K}$ is the small-scale fading channel coefficient.

Since the objective of this work is to minimize the number of RIS elements, i.e., the overall RIS area, to reduce configuration time, the channel gains must account for both the transmitter and RIS areas as functions of the number of antenna elements. Thus, β_k is modeled as a function of the transmitter and receiver antenna areas, as described in [31]

$$\beta_k = \frac{A_t A_U}{(\lambda d_{BU})^2} \ , \tag{9}$$

where A_t is the transmitter antenna arrea, A_t can be expressed as $A_t = M \times A_{\text{MIMO}}$, where A_{MIMO} denotes the area of a single antenna element. Similarly, A_U corresponds to the area of a single receiver antenna element. In this work both A_{MIMO} and A_U are set to have an area of $\left(\frac{\lambda}{2}\right)^2$. Additionally, d_{BU} is the distance between the BS and the user.

The optimal beam, selected to establish the best link to the user at a given location, is determined as follows [6]

$$\mathbf{f}^{\star}_{\text{los},k} = \underset{\mathbf{f}\in\mathbf{F}}{\text{argmax}} \frac{1}{K}\sum_{k=1}^{K}\log_2\left(1+\rho\left|\mathbf{G}_{\text{los},k}\mathbf{f}\right|^2\right) \ , \tag{10}$$

where ρ represents the power-to-noise ratio, defined as $\frac{P_t}{\sigma^2}$ with P_t being the transmitted power. Based on this equation, the achievable rate R is evaluated as follows [29]

$$\text{R}_{\text{los}} = \frac{1}{K}\sum_{k=1}^{K}\log_2\left(1+\rho\left|\mathbf{G}_{\text{los},k}\mathbf{f}^{\star}_{\text{los},k}\right|^2\right) \ . \tag{11}$$

D. VLoS Channel Model

Whenever a blockage event is detected by the VAWC framework, an RIS-assisted link is utilized to perform a PHO [8]. The signal received through the RIS beam can be expressed as

$$y_{\text{VLoS}} = (\mathbf{v}^{\star})^H\mathbf{G}_{\text{VLoS}}\mathbf{f}^{\star}_{\text{BI}}s_{\text{VLoS}} + n_{\text{VLoS}} \ , \tag{12}$$

where, s_{VLoS} reresents the transmitted symbol through the VLoS link, $(\mathbf{v}^{\star})^H\mathbf{G}_{\text{VLoS}}\mathbf{f}^{\star}_{\text{BI}}$ denotes the total cascaded end-to-end channel from the BS to the blocked user through the RIS, $\mathbf{f}^{\star}_{\text{BI}}$ represents the optimal beam from the BS to the RIS, and $\mathbf{v}^{\star}$ denotes the optimal RIS steering vector that maximizes R. Additionally, H refers to the Hermitian transpose operation [21] [32].

In order to capture a practical system performance we adopt the scenario mentioned earlier in section I where the link from the BS to RIS falls in the far-field model and the link from the RIS to the user falls in the near-field model thus $\mathbf{G}_{\text{VLoS}}$ is comprised of two channel gains. The first characterizes the link from the BS to the RIS and is expressed by the far-filed model similar to the equation (9) as follows

$$\beta_{BI} = \frac{A_t A_{\text{RIS}}}{(\lambda d_{BI})^2} \ , \tag{13}$$

A_{RIS} is the RIS area and is expressed as $A_{\text{RIS}} = N \times A$, where A represents the area of a single RIS element, and d_{BI} is the distance between the BS and the RIS [30].
For the second part of the cascaded channel, specifically the link from the RIS to the blocked user, the channel is assumed to be in the near-field model and can be expressed as [31]

$$\beta_{IU} = \frac{4A_{\text{RIS}}}{3\lambda^2}\left(\frac{\sqrt{2\left(\frac{(d_{IU})^2}{A_U}\right)}}{\sqrt{1+2\left(\frac{(d_{IU})^2}{A_U}\right)}\left(1+4\left(\frac{(d_{IU})^2}{A_U}\right)\right)} + 2\cot^{-1}\left(\sqrt{8\left(\frac{(d_{IU})^2}{A_U}\right)\left(1+2\frac{(d_{IU})^2}{A_U}\right)}\right)\right) \ , \tag{14}$$

here, d_{IU} represents the distance from the RIS to the blocked user. Therefore, the final channel coefficients of the cascaded channel G_{VLoS} can be expressed as

$$\mathbf{G}_{\text{VLoS,k}} = \sqrt{\beta_{IU}\beta_{BI}}\mathbf{h}_{c,k}e^{\left(j2\pi\frac{k(d_{\text{RIS}}+d_{\text{MIMO}})}{K\lambda}\right)}f(\theta,\phi), \tag{15}$$

where $\mathbf{h}_{c,k}$ is the small-scale fading coefficient for the cascaded channel. In our work, we assume perfect CSI however, our primary focus is on capturing the impact of large-scale fading in the near-field, where path loss becomes the dominant factor influencing the required number of RIS elements. Instead of employing high-resolution angle-dependent beamforming for near-field modeling which introduces substantial computational complexity we focus on large-scale fading. This

Symbol	Definition
M	Number of ULA MIMO elements
N	Number of IRS elements
f , v	BS, IRS predefined beams vectors
K	Number of OFDM subcarriers
P_t	Transmitted power
ρ	Power-to-noise ratio
λ	Carrier wavelength
G	Channel gain parameter
β , h	Large and small scale fading parameters
$f(\theta, \phi)$,	Function of angles of arrival and departure
θ , ϕ	Azimuth and elevation angles
A_T	MIMO ULA array area
A_{RIS}	RIS grid area
A	RIS element area
A_{MIMO}, A_U	Antenna element area for MIMO and user
d	Antenna element spacing
d_{BI}	Distance from BS to RIS
d_{IU}	Distance from RIS to user
R	Achievable rate
B	Number of didoes per RIS elements
C_{lk}	Shift register clocking rate
T_c	RIS configuration time
T_W^{RIS}	Waiting time before triggering PHO

Table I: Key notation used in system and channel models.

choice is motivated by the fact that computational complexity is directly related to the codebook size, as discussed in the computational complexity section of the paper. The achievable rate of the RIS VLoS link can be expressed as

$$\mathrm{R}_{\mathrm{VLoS}} = \frac{1}{K}\sum_{k=1}^{K}\log_2\left(1+\rho\cdot\left|(\mathbf{v}^{\star})^H\mathbf{G}_{\mathrm{VLoS},k}\mathbf{f}_{\mathrm{BI}}^{\star}\right|^2\right). \quad (16)$$

III. Problem formulation and suggested optimization

The main objective of this work is to minimize the number of RIS elements N, and subsequently the RIS configuration time T_c, in order to reduce the signal processing complexity BT overhead, while maintaining the desired achievable rate. Striking a balance between minimizing N and preserving the required link performance is essential to ensure efficient and timely execution of the PHO process. This trade-off is particularly critical for enabling RIS-assisted links to support time-sensitive applications, such as autonomous driving and real-time user tracking.

A. Problem Formulation

The purpose of the optimization process presented in this work is to determine the optimal configuration for the end-to-end RIS-assisted system, taking into account key parameters such as the number of dedicated subcarriers K, the transmitter specifications represented by the number of antenna elements M, the transmission power, and the selection of optimal beamforming vectors from the BS to the RIS and from the RIS to the blocked user.

This study investigates the optimization of the number of RIS elements under two distinct scenarios. In the first scenario, the RIS is assumed to be equipped with ideal continuous phase shifters, enabling highly accurate beam steering with minimal directivity losses. This idealized model offers reduced computational complexity and serves as a theoretical benchmark. In contrast, the second scenario considers a more practical deployment in which the RIS employs discrete phase shifters. In this case, the configuration is influenced by the number of diodes per RIS elelemnt B, which governs both the number of available RIS beamforming patterns and the number of bits required to configure the RIS. Although this scenario introduces increased computational overhead, it reflects real-world hardware limitations more accurately. These two scenarios collectively provide insights into the trade-off between computational complexity and practical feasibility in RIS-assisted mmWave systems. Based on that, the optimization problem is formulated for each scenario as follows.

*1) **Scenario 1**:* The RIS has an ideal continuous phase shifter. By substituting equations (13), (14), and (15) into equation (16), the achievable rate can be expressed as

$$\mathrm{R}_{\mathrm{VLoS}} = \frac{1}{K}\sum_{k=1}^{K}\log_2\left(1+\rho MN^2C\left|\mathbf{h}_{c,k}\mathbf{f}_{\mathrm{BI}}^{\star}\right|^2\right), \quad (17)$$

where the beam $\mathbf{f}_{\mathrm{BI}}^{\star}$ is selected to maximize the RIS link SNR for the blocked user [6]

$$f_{\mathrm{BI}}^{\star} = \underset{f_{\mathrm{BI}}\in\mathcal{F}}{\operatorname{argmax}}\frac{1}{K}\sum_{k=1}^{K}\log_2\left(1+MN^2C\rho\left|h_{c,k}f_{\mathrm{BI}}\right|^2\right), \quad (18)$$

where

$$C = \frac{4A^2A_{\mathrm{MIMO}}}{3\lambda^4d_{\mathrm{BI}}^2}\left(\frac{\sqrt{2Q}}{\sqrt{1+2Q}\,(1+4Q)} + 2\cot^{-1}\left(\sqrt{8Q\,(1+2Q)}\right)\right) \times e^{j2\pi\frac{k(d_{\mathrm{RIS}}+d_{\mathrm{MIMO}})}{K\lambda}}, \quad (19)$$

where $Q = \frac{d_{\mathrm{IU}}^2}{A_U}$. As part of the continuous phase shifter assumption, the RIS beamforming vector $\mathbf{v}^{\star}$ is assumed to effectively counteract the values generated by $f(\theta,\phi)$ in equation (15). Through mathematical manipulation of equation (17) a function in terms of N can be found as

$$N = \left(\frac{2^{RK}}{\prod_{k=1}^{K}MC\rho\left|h_{c,k}f_{\mathrm{BI}}^{\star}\right|^2}\right)^{\frac{1}{2K}}, \quad (20)$$

and subsituting (20) in equation (4) the objecctive function to minimize T_c can be expressed as follows:

$$\text{(P1)}: \quad \min_{M,K,f_{\mathrm{BI}}^{\star}} \quad T_c = \frac{B}{C_{lk}}\left(\frac{2^{RK}}{\prod_{k=1}^{K}MC\rho\left|h_{c,k}f_{\mathrm{BI}}^{\star}\right|^2}\right)^{\frac{1}{2K}} \quad (21)$$

subject to:

$$R \geq R_{\mathrm{th}}, \quad (21.a)$$

$$M_{\min} \leq M \leq M_{\max}, \quad (21.b)$$

$$P_{\min} \leq P_t \leq P_{\text{budget}}, \tag{21.c}$$
$$1 \leq K \leq K_{\max}, \tag{21.d}$$

*2) **Scenario 2**:* The RIS is equipped with a discrete phase shift, where the number of available beams is dependent on B

$$\mathbf{v} = \text{DFT}(2^B)\ , \tag{22}$$

where $\text{DFT}(2^B)$ refers to the discrete Fourier transform function for RIS beamforming. In this case, the achievable rate can be expressed as

$$\text{R}_{\text{VLoS}} = \frac{1}{K}\sum_{k=1}^{K}\log_2\left(1+\rho MN^2C\left|(\mathbf{v}^\star)^H\mathbf{h}_{c,k}\mathbf{f}_{\text{BI}}^\star\right|^2\right)\ , \tag{23}$$

where the pair of beams $\mathbf{f}_{\text{BI}}^\star$ and $\mathbf{v}^\star$ are selected to maximize the RIS link SNR for the blocked user [21] [32]

$$(\mathbf{v}^\star, \mathbf{f}_{\text{BI}}^\star) = \underset{\mathbf{f}\in\mathcal{F},\mathbf{v}\in\mathcal{V}}{\text{argmax}}\frac{1}{K}\sum_{k=1}^{K}\log_2\left(1+\rho\left|(\Omega^T\otimes\mathbf{f}_{\text{BI}})\mathbf{G}_{\text{VLoS},k}\right|^2\right)\ , \tag{24}$$

where $\Omega = \text{diag}(\mathbf{v})$, and $\otimes$ denotes the Kronecker product operation [33], hence the objective function for T_c can be determined from equations (4) and (23) as follwos

$$\text{(P2)}: \min_{M,K,f_{\text{BI}}^\star,v^\star} \quad T_c = \frac{B}{C_{lk}}\left(\frac{2^{RK}}{\prod_{k=1}^{K}MC\rho\left|(v^\star)^H h_{c,k}f_{\text{BI}}^\star\right|^2}\right)^{\frac{1}{2K}} \tag{25}$$

subject to:

$$R \geq R_{\text{th}}, \tag{25.a}$$
$$M_{\min} \leq M \leq M_{\max}, \tag{25.b}$$
$$P_{\min} \leq P_t \leq P_{\text{budget}}, \tag{25.c}$$
$$1 \leq K \leq K_{\max}. \tag{25.d}$$

It is worth mentioning that equations (18) and (24) in both scenarios do not represent constraints, but rather internal beam selection rules that must be employed to maximize the SNR during the evaluation of the objective function. The optimal beams $\mathbf{f}_{\text{BI}}^\star$ and $\mathbf{v}^\star$, selected through this process, directly influence the achievable rate and thereby contribute to minimizing the number of RIS elements required to establish a reliable link. Thus, in each iteration of the optimization process, the selection of the optimal beams follows the steps outlined in (Algorithm 1). The process begins by setting the transmitter and RIS specifications, followed by the calculation of the optimal beams. Further details of the optimization approach are provided in the following section.

The objective function and its associated constraints are designed to minimize the configuration time for establishing an RIS-assisted link by indirectly reducing the required number of RIS elements needed to achieve a target data rate. This is accomplished by selecting the optimal combination of transmitter MIMO antenna size, allocated OFDM subcarriers, and RIS beamforming vectors to maximize the effective SNR across all subcarriers. The constraints enforce practical limitations, such as meeting minimum data rate requirements, respecting hardware and power limitations, and selecting beams from discrete codebooks that best align with the propagation environment.

Algorithm 1 Selecting optimal BS & RIS beams to minimize T_c

1: **Input:** MIMO transmitter antenna range $M_{\min}, M_{\max}$, RIS resolution B, and other system parameters
2: **for** each iteration **do**
3: Set transmitter antennas M
4: Compute BS MIMO beamforming codebook size: $\mathcal{F}$
5: Compute RIS beamforming codebook size: $\mathcal{V}$
6: Calculate optimal beam $f_{\text{BI}}^\star$ using equation (18)
7: Calculate optimal RIS beam $v^\star$ using equation (24)
8: Evaluate T_c using the objective functions in (21) or (25) based on the considered scenario
9: **end for**
10: **Output:** Optimal configuration $\mathbf{f}_{\text{BI}}^\star$ and $\mathbf{v}^\star$ for minimizing T_c

The optimization problems formulated in equations (21) and (25) are both non-convex because of variables such as K and $f_{\text{BI}}^\star$ are discrete in nature, while others like ρ can be considered continuous, resulting in a mixed-variable domain. Also, the beam selection functions presented in (18) and (24) are both non-convex. These properties render traditional gradient-based or convex solvers unsuitable for this scenario.

B. Proposed optimization algorithm

This work is the first to explore the concept of environment-aware RIS-assisted PHO, establishing a foundational baseline for future research directions such as proactive user tracking to address the limitations associated with the passive nature of RIS technology. The optimization is performed in an offline approach to construct a site-specific CKM, thereby ensuring that the algorithm's convergence time does not impact real-time system responsiveness. The CKM enables a fast RIS configuration setup selection to steer the signal toward the predicted blockage location in online scenarios. This approach enables efficient and timely handover execution. Future research may involve periodic updates to the CKM using ML prediction techniques and digital twin models to further enhance accuracy in highly dynamic mmWave environments.

Metaheuristic optimization methods have become a natural choice for effectively handling non-convexity and mixed-variable system models. These algorithms do not rely on gradient information and can explore large and complex solution spaces for suboptimal solutions. Among various metaheuristic methods such as genetic algorithms (GA), simulated annealing (SA), and ant colony optimization (ACO), Particle Swarm Optimization (PSO) stands out as particularly well-suited for this problem.

PSO offers several advantages in this context. It is simple to implement, requiring fewer hyperparameters than GA or SA, and due to this fact it exhibits faster convergence time per iteration. Moreover, PSO leverages swarm intelligence by balancing individual particle exploration and global exploitation, which improves the search for the best suboptimal solution.

PSO is an effective optimization algorithm widely employed for solving complex problems involving multiple parameters and of a discrete nature. The use of PSO has been applied to optimize the states of the RIS elements for uniform phase change [34], [35], and to optimize the spacing of RIS elements [25] [36].

In this work, we propose the use of PSO to achieve the desired trade-off between minimizing the number of RIS elements while maintaining the desired link rate, leading to estimating the RIS configuration time T_c. The optimizer identifies the optimal parameters, such as K, P_t, M, and the optimal beams $\mathbf{v}^\star$ and $\mathbf{f}_{\text{BI}}^\star$ by following the steps outlined in (Algorithm 2) and the proposed algorithm is used to solve ($\mathbf{P1}$) and ($\mathbf{P2}$) depending on the scenarios considered.

The algorithm begins by setting the maximum number of iterations and the number of particles that will explore both the local and global solutions within the solution space of the parameters. The first step is to find the optimal transmitter specifications represented by M. At the start of each iteration, the algorithm initializes the population of particles at random positions to search in parallel across the entire solution space. The particles randomly select M, which represents the required number of ULA transmitter elements needed to establish a link with the desired R. The number of transmitter antenna elements M is selected from a range bounded by M_{min} and M_{max}. Within this range, M is discretized into fixed block sizes of 16, 32, 64, and so on, up to M_{max}. For instance, if the maximum number of available transmit antennas is set to 64, the possible values for M would be 16, 32, and 64. In this work, the optimization process is conducted for three different values of M_{max}, specifically 128, 256, and 512, each offering a distinct set of discrete options for M. These variations allow for evaluating the impact of transmitter array size on system performance and RIS-assisted link efficiency.

To define the transmit power P_{t} utilized by the transmitter, we focus on optimizing $\rho = \frac{P_{\text{t}}}{\sigma^2}$. Various values of ρ have been considered in the literature, such as $\rho = 5$ dB in [9]. In this study, we assume that the minimum transmitter configuration, M_{min}, corresponding to a 16-element antenna block, achieves a baseline of $\rho = 0$ dB. As the algorithm increases the number of transmitter elements to the next block size (e.g., $M = 32$), the available transmit power budget is adjusted to improve ρ, allowing values from 0 dB up to 3 dB. More generally, each doubling of M results in a 3 dB increase. This strategy aligns with the physical interpretation that increasing the array size enhances directional gain, thereby improving ρ. Accordingly, the optimization algorithm evaluates all possible combinations of M and transmit power for each M_{max}, ultimately selecting the configuration that provides the most favorable trade-off between link quality and power consumption.

The next step involves calculating the best beamforming codebook vector, $\mathbf{f}_{\text{BI}}$, used for transmission from the BS to the RIS. These calculations are based on the randomly selected M positions. Additionally, depending on the user location and the value of B, the algorithm calculates $\mathbf{v}$, which represents the best beam used to transmit from the RIS to the blocked user.

The initial value of the number of subcarriers, K, is set to 1 and is incremented cautiously due to the associated computational complexity. To constrain the system complexity and maintain practical feasibility, a threshold is introduced, limiting the maximum number of RIS elements to 1000. This threshold is based on our previous findings in [8], where 1000 elements were required to establish a reliable RIS-assisted link for a PHO. In the present work, the primary objective is to reduce the required number of RIS elements N while achieving comparable performance. Once the algorithm computes N using the current values of system parameters, it compares the result against the defined threshold. If the computed value exceeds the threshold, K is incremented, and the process is repeated to recompute N. This iterative procedure continues until the condition $K \leq K_{\text{max}}$ is satisfied, ensuring that the optimal combination is selected to minimize N without exceeding the maximum permissible complexity.

Algorithm 2 PSO for RIS configuration time.

Choose population size *num_particles*, number of iterations, inertia weight *w*, cognitive coefficient *c1*, and social coefficient *c2*.
Initialize the subcarriers values with $K = 1$ and set the value of K_{max} and B.
Set the threshold value of RIS elements when exceeded K is incremented afterwards.
Set the minimum M_{min} and maximum M_{max} values for *M* with increment of multiples of (block size).
Initialize particle positions *M* as random multiples of the block size within the range $[M_{\text{min}}, M_{\text{max}}]$.
Initialize P_t depending on the selected MIMO block between [*P_min*, *P_max*]
for iter = 1 to *num_iterations* **do**
  for each particle from *num_particles* **do**
    Evaluate Calculate $\mathbf{f}_{\text{BI}}$,$\mathbf{v}$.
    Evaluate *N* and RIS square area.
    if *N* exceeds of threshold RIS elelments. **then**
      Increment *K*
    end if
    if current N value is better than best local value **then**
      Update best local values (N,*M*, P_t,K ,$\mathbf{f}_{\text{BI}}$,$\mathbf{v}$).
    end if
    if current N value is better than global best value **then**
      Update global best values (*M*, P_t,K ,$\mathbf{f}_{\text{BI}}^\star$, $\mathbf{v}^\star$).
    end if
  end for
  for each particle **do**
    Update velocities PSO velocity update equations.
    Update particle positions and ensure values remain within ranges.
    if *K* exceeds K_{max} **then**
      Set *K* to K_{max}.
    end if
  end for
end for
return Optimized N, T_c, Best values : M, $\mathbf{f}_{\text{BI}}^\star$, $\mathbf{v}^\star$, K, P_t.

At this stage, the best personal (local) value of N is updated based on the minimum value across all particles. The global best position is also updated to achieve the minimal N across all iterations, which is then returned as the optimized N. Additionally, the algorithm determines the optimal set of parameters required to achieve the desired R at the optimized N. These include the required transmitter array M, the optimal BS beam $\mathbf{f}_{\text{BI}}^{\star}$ transmitting to the RIS, the optimal RIS beam $\mathbf{v}^{\star}$ transmitting to the user, and the best number of subcarriers allocated for the user.

It is important to note that equations (14) and (20) are derived based on the approximation of a squared array area [31]. Consequently, the optimization process involves determining the optimal N. Since the optimized N may not yield a perfect square area, it is approximated to the nearest square area of then T_c is calculated. Further details about the area approximation are provided in the results section.

C. Computational complexity

The computational complexity associated with minimzing T_c depends on the considered scenario. In the continuous phase shift, the RIS beamforming vector is analytically derived to counteract the angle-of-arrival and angle-of-departure components, eliminating the need for RIS optimal beam search. The complexity in this case primarily arises from evaluating the achievable rate over a finite set of transmit-side beams $\mathcal{F}$, resulting in a complexity on the order of $\mathcal{O}(|\mathcal{F}| \cdot K)$, where K is the number of allocated subcarriers to a blocked user.

In contrast, the discrete phase shift scenario requires joint optimization over quantized RIS beams and transmit beams, typically from codebooks of sizes $|\mathcal{V}|$ and $|\mathcal{F}|$, respectively. The joint beam search thus incurs a complexity of $\mathcal{O}(|\mathcal{V}| \cdot |\mathcal{F}| \cdot K)$, which grows significantly with beam resolution. Therefore, while the continuous case offers lower computational overhead, the discrete case requires exhaustive or heuristic search over a larger beam codebook solution space, making it computationally more demanding.

IV. Suggested RIS-Assisted PHO Framework

In this work, the bus in Fig. 2 prevents ULA sector 1 from establishing a LoS link to the user. When this blockage event is detected by the VAWC framework integrated with the BS, it triggers a PHO to ULA sector 2's RIS-assisted link. The new RIS-assisted link will be selected from a subset of VLoS beam indices stored at the BS as part of the RIS-assisted CKM database (see Fig. 1).

The PSO algorithm determines the optimal M used in ULA sector 2 and the optimal N for the RIS required to establish the link to the blocked area based on the desired rate. Additionally, the RIS-assisted CKM contains the optimal parameters, calculated based on the outcome of the PSO algorithm performed using an offline estimation approach, to enable a fast response during online scenarios. These parameters include the optimal beams $\mathbf{f}_{\text{BI}}^{\star}$, $\mathbf{v}^{\star}$, and the corresponding transmitted power to the blocked location. Finally, the PSO algorithm will determines T_c based on the optimized value of N, and T_c will be incorporated as an additional time to execute the updated PHO timing requirements, as shown in Equation (3), ensuring a smooth and accurate timing to trigger the PHO procedure.

V. Performance Evaluation and Results

The work in this paper adopts the simulation environment described in [8], where the VAWC framework detects blockage events, user locations, and obstacle locations as explained in the next section.

A. Simulation Environment

The simulation environment is based on the colocated camera blockage scenario presented in the dataset [29]. Below are the key notes of the simulation environment:

- The VAWC system monitors a 90×15-meter street, where the length of the street aligns with the x-axis, and the width corresponds to the y-axis. The street is located in the xy plane at $z = 0$, with the point of origin at the upper right corner of the street, as shown in Fig. 2.
- A BS is positioned at $(x = 45)$ at mid point of the 90 street. The BS, set at a height of 5 meters, is equipped with cameras providing a panoramic view of the street. An RIS supports the BS mounted on a building behind it, located at $(45, -5)$ with a height of 6 meters. The blockage is modeled by a bus obstructing the LOS link in certain segments of the street.
- The pre-established CKM enables the RIS to steer the signal to the car shown in Fig. 2. The car lane is represented as a straight-line trajectory at $y = 9$, extending from the point $(0, 9)$ to the point $(90, 9)$.
- Depending on the user's location and movement speed, the VAWC in [6] determines the optimal time to trigger a PHO based on T_W in equation (1). In this work, we propose a new time to trigger the PHO, represented by $T_{\text{W}}^{\text{RIS}}$ as presented in equation (3), which accounts for T_c of the optimized RIS area.

In this simulation, we focused on a section of the street experiencing signal blockage, specifically between $x = 15$ and $x = 22$ meters. The RIS is dedicated to providing coverage for this segment of the street.

B. Simulation Results

The proposed algorithm computes the optimal values of N and T_c. As discussed previously, equations (14), (20), and (25) are derived under the assumption of a squared array area approximation, as outlined in [31]. Accordingly, the optimization process entails identifying the optimal N, which may not always correspond to a perfect square. In such cases, the algorithm approximates the result to the nearest perfect square to facilitate practical deployment. An illustration of this procedure is shown in Fig. 5(a). Under the ideal continuous phase shifter scenario, the optimal number of RIS elements across various locations within the coverage area was found to range from 345 to 350 elements, depending on the user's position. Since these values do not form a perfect square, the algorithm approximates them to $N = 361$ elements, arranged in a 19×19 square grid, to ensure structural compatibility

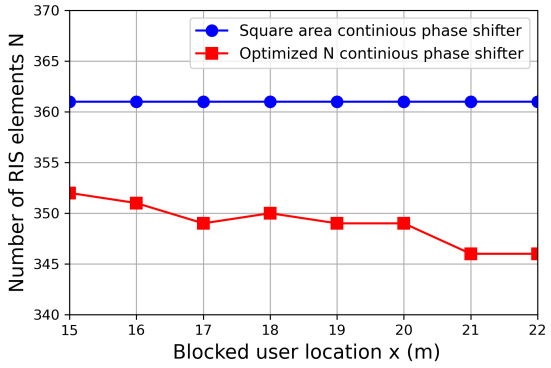

(a) Optimized N and approximated RIS square area, continuous phase shifter scenario.

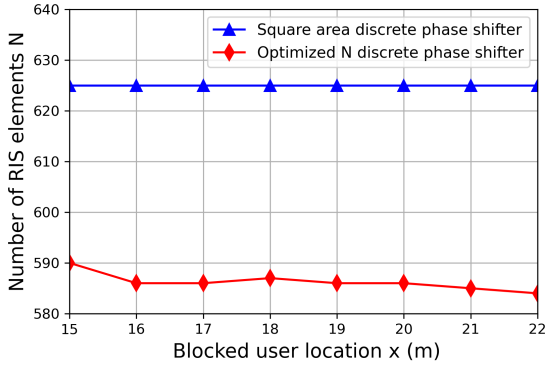

(b) Optimized N and approximated RIS square area, discrete phase shifter scenario $B = 3$.

Figure 5: Comparative plots of RIS square area and Optimized N for both continuous and discrete phase shifter scenarios.

and performance consistency. It is also worth mentioning that when the blocked user is closer to the BS located at $x = 45$, fewer RIS elements are required. This is clearly demonstrated in the optimized N graph, where the user at $x = 15$ requires more RIS elements than the user at $x = 22$, as it is farther from the BS.

In the second scenario, which assumes the use of a discrete phase shifter with a resolution of $B = 3$ bits, the optimal values of N were found to range from 585 to 600. The algorithm then approximates this range to $N = 625$, corresponding to a square grid of 25×25 elements. The results presented in Fig. 5(b) demonstrate that while the ideal continuous phase shifter offers a lower number of required elements and faster computational convergence, it may result in impractical deployment scenarios. Nonetheless, the reduced computational complexity makes this scenario more suitable for real-time or online estimation applications.

The results presented in Fig. 6 illustrate the impact of subcarrier allocation on the required RIS area to achieve a target link rate R. The optimization algorithm identifies two viable configurations: a larger RIS with fewer allocated subcarriers or a smaller RIS supplemented by a greater number of subcarriers. This trade-off is evaluated at various locations along the street, as shown in the figure. For instance, at

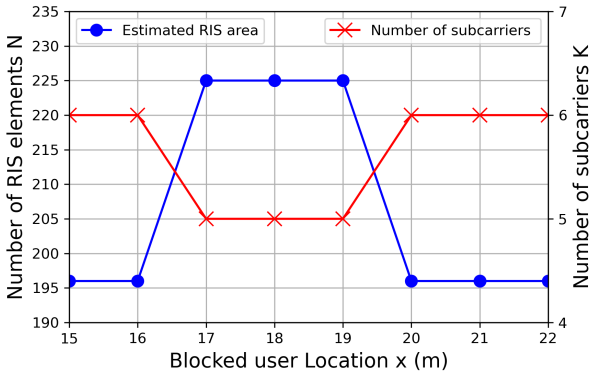

Figure 6: Trade-off between RIS area and number of subcarriers for the same achievable rate $R_{\text{th}} = 1$ (continuous phase shifter scenario).

location $x = 16$, the optimized RIS size is $N = 196$ elements with $K = 6$ subcarriers. Conversely, at location $x = 19$, the algorithm selects a larger RIS with $N = 225$ elements while reducing the subcarriers to $K = 5$. These findings underscore the influence of subcarrier allocation on RIS-assisted link efficiency. Allocating a greater number of subcarriers can compensate for a reduction in RIS size while maintaining the required link performance. This results in faster RIS configuration times and reduced signal processing complexity, owing to the deployment of fewer RIS elements for establishing the VLoS link.

Fig. 7 is consistent with the preceding results, illustrating the required RIS area and the corresponding subcarrier allocation across various segments of the blocked region. Fig. 7(a) depicts the variation in RIS area with respect to different achievable rate targets. The estimated square RIS areas range from $N = 289$ elements, arranged in a 17×17 grid for the lowest achievable rate of $R = 1$, up to $N = 841$ elements, arranged in a 29×29 grid for the highest rate of $R = 6$. Fig. 7(b) presents the associated subcarrier allocations required for each RIS configuration to maintain the same achievable rate. For $R = 1$, the number of allocated subcarriers varies between $K = 11$ and $K = 12$, depending on the RIS area, whereas for $R = 6$, the required number of subcarriers reaches $K = 24$. It is worth mentioning that, the proposed algorithm was able to achieve higher rates with the same RIS area by increasing the allocated subcarriers. This is represented by the overlap of the $R = 2$ and $R = 3$ curves in Fig. 7(a). However, for higher rates, both the RIS area and the allocated subcarriers needed to be increased in order to achieve the desired R.

These findings highlight an important trade-off: the allocation of additional subcarriers can compensate for a reduction in RIS area to achieve a given target rate, and vice versa. This enables the system to flexibly balance between hardware complexity and signal processing load. Consequently, once the RIS area is fixed to meet configuration time constraints, dynamic subcarrier allocation can be employed to acquire the achievable rate based on user demands without requiring physical modifications to the RIS structure.

The results in Fig. 8 highlight another factor that contributes to minimizing the RIS area: the use of narrower beams

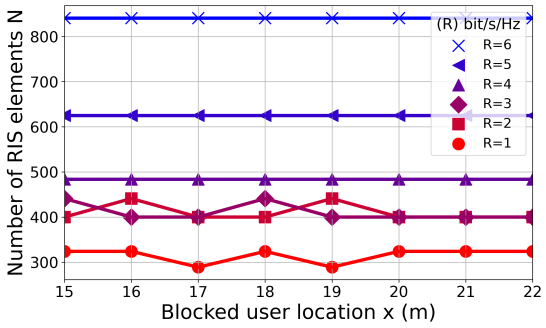

(a) Effect of RIS area on the achievable rate

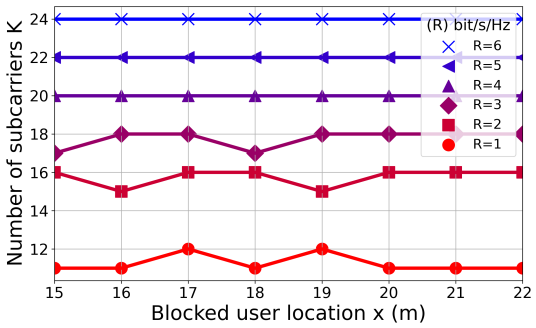

(b) Effect of subcarriers on the achievable rate

Figure 7: Comparative plots of RIS area and subcarrier effects on achievable rates (discrete phase shifter $B = 3$, $M = 512$).

projected onto the RIS by increasing the number of transmitter MIMO elements. This figure illustrates the correlation between the number of subcarriers K, the number of transmitter MIMO elements M, and the required RIS area for different values of R. In general, increasing the number of MIMO elements enhances performance. A comparison of $M = 128$, $M = 256$, and $M = 512$ shows that a transmitter with $M = 512$ requires a smaller RIS area to achieve the same data rate, particularly noticeable at $K = 6$. Another perspective on the impact of the transmitter MIMO can be observed for $R = 1$, where both $M = 512$ and $M = 256$ share the same RIS area. However, the $M = 512$ transmitter requires only four subcarriers to achieve the required link rate, whereas the $M = 256$ transmitter requires five subcarriers. Overall, larger MIMO arrays consistently deliver better performance while reducing the need of other resources, either by reducing the required number of subcarriers or by minimizing the RIS area.

Fig. 9 illustrates the relationship between the RIS configuration time T_c and the performance of the RIS-assisted link, evaluated in terms of the achievable rate R and the required RIS area necessary to attain that performance level. The configuration time is estimated based on a shift register operating at a clocking rate of $C_{lk} = 100\,\text{kHz}$ [10]. Fig. 9(a) presents the performance results for the continuous phase shift scenario under varying target rates. For the lowest achievable rate ($R = 1$), a RIS composed of $N = 225$ elements is sufficient, resulting in a configuration time of approximately

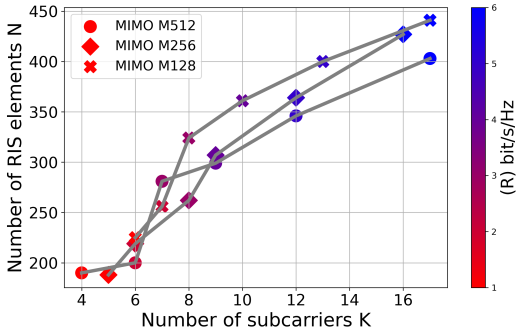

Figure 8: Effect of transmitter MIMO on achievable rate, RIS area, and subcarriers (continuous phase shifter scenario).

$T_c = 2\,\text{ms}$. Conversely, to achieve the highest rate ($R = 6$), the required RIS area increases to $N = 441$ elements, yielding a configuration time of approximately $T_c = 9\,\text{ms}$. These results underscore the importance of minimizing the RIS area to achieve faster configuration responses, which is critical for latency-sensitive applications such as autonomous vehicular communication. Hence, optimizing the RIS configuration to use the smallest feasible number of elements becomes essential in such scenarios.

Similarly, Fig. 9(b) presents the results of the optimization algorithm under the discrete phase shifter scenario with $B = 3$. In this case, achieving the lowest rate ($R = 1$) requires a larger RIS area of $N = 324$ elements compared to the continuous phase shift scenario, resulting in a configuration time of approximately $T_c = 10\,\text{ms}$. To support the highest rate ($R = 6$), the required RIS area increases significantly to $N = 841$ elements, yielding a configuration time of approximately $T_c = 25\,\text{ms}$. These findings indicate that while modeling the RIS under a continuous phase shifter assumption can reduce computational complexity, it considerably underestimates the minimum RIS size required to sustain reliable link performance. Accurately mapping the RIS area and the corresponding configuration time is essential not only for achieving the desired link rate but also for ensuring seamless handover timing, particularly in mobile scenarios. Although the continuous phase assumption may be advantageous for real-time estimation due to its simplicity, relying solely on this approximation in practical deployments may result in connection interruptions and degraded link quality.

Based on the findings presented above, the required RIS area to achieve the highest rate is $N = 841$, corresponding to a configuration time of $T_c = 25\,\text{ms}$. To account for the impact of the RIS configuration time on the PHO framework discussed in [8], the original T_W value estimated in [6] must be updated to $T_{\text{W}}^{\text{RIS}}$, as detailed in equations (2) and (3). For instance, in [6], a scenario is considered where a blocked user, represented by a vehicle, moves towards the blockage area at a speed of 10 miles per hour. The original estimation of $T_W = 4.7$ seconds was provided before triggering handover to a second BS. IN our work, to ensure accurate triggering of the PHO by an RIS-assisted link instead of a second BS, the updated value $T_{\text{W}}^{\text{RIS}}$ must be used, which accounts

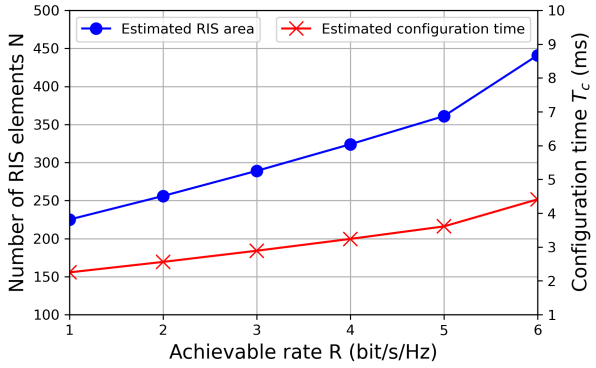

(a) Configuration time of RIS (continous phase shifter).

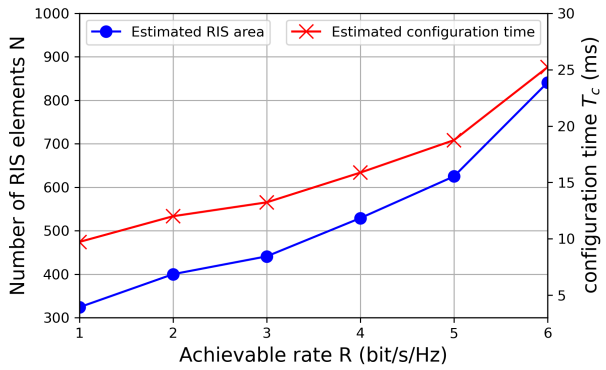

(b) Configuration time of RIS (discrete phase shifter $B = 3$)

Figure 9: Comparative plots of achievable rates effects RIS area and configuration time.

Table II: Updated triggering time for PHO from The Work in [6] with constant car Speed Of 10mph

RIS Area	R (bit/s/Hz)	T_c (ms)	T_W^{RIS} (s)
324	1	9.72	4.69028
400	2	12.00	4.68800
441	3	13.23	4.68677
529	4	15.87	4.68413
625	5	18.75	4.68125
841	6	25.23	4.67477

for the additional timing constraint introduced by the RIS configuration response. In the case of considering an RIS-assisted link established by an RIS with an area of 841 elements, ensuring link performance of $R = 6$, the RIS configuration time is $T_c = 25$ ms, leading to an updated value for $T_{\text{W}}^{\text{RIS}} = 4.67477$ s. This value can be used by the RIS-assisted PHO framework to trigger the handover accurately.

Table II presents the optimal handover triggering time, accounting for the RIS configuration response. The listed RIS areas correspond to different achievable rates. For an RIS area of 841 elements, the PHO algorithm can safely trigger the process with sufficient timing margin, ensuring the RIS-assisted link achieves an achievable rate of $R = 6$. The remaining user movement speeds and their corresponding T_W values from [6] can be updated in a similar manner.

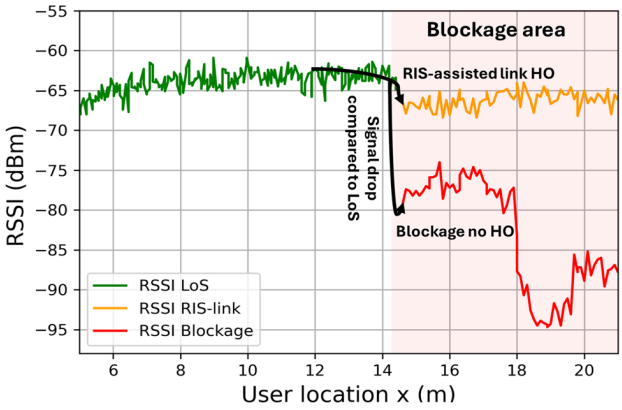

Figure 10: Comparison of RSSI for LoS, RIS-assisted, and Blockage scenarios with and without RIS.

Finally, in our previous work [8], performance analysis was conducted for RIS-assisted links in the context of RIS-assisted PHO. The estimated number of RIS elements required to achieve acceptable link performance during a handover to a blocked user was $N = 1000$, with the received signal strength indicator (RSSI) used as the primary evaluation metric.

The results in Fig. 10 present a comparison between three scenarios: (i) the RSSI of the LoS signal, where no blockage impedes the BS from establishing a direct link to the user; (ii) the RSSI of the RIS-assisted link, where a beam is steered from the RIS to the blocked area using parameters optimized by the proposed PSO algorithm, denoted as the *RSSI RIS-link* curve; and (iii) the RSSI values in a blocked scenario without RIS, denoted as the *RSSI Blockage* curve. While the RIS-assisted link shows reduced signal strength compared to the LoS case, it significantly outperforms the blocked scenario without RIS, improving the RSSI by approximately 15 to 30 dBm, depending on blockage severity and user location. The proposed PSO algorithm reduces the required RIS area from $N = 1000$, based on our findings in [8], to $N = 841$, achieving a 15% reduction in the number of RIS elements required to establish the link. This reduction is attained without compromising performance and while enhancing the RSSI relative to the blocked scenario. Moreover, minimizing the RIS area results in faster configuration response, enabling timely beam steering toward the blocked region. By explicitly calculating and incorporating the RIS configuration time into the handover process, the PHO can be triggered more accurately, ensuring uninterrupted service for blocked users, an essential improvement not addressed in our previous work.

VI. Conclusion

This work presents a novel RIS-assisted VAWC framework capable of providing seamless coverage by restoring blocked LoS links in mmWave networks. It further enhances PHO procedures by minimizing the number of RIS elements to ensure faster RIS configuration response. The proposed approach facilitates accurate PHO-triggered handovers, improving mmWave signal reliability in obstructed scenarios. The

optimization process identifies the optimal system configuration to maximize the achievable rate. The results demonstrate a trade-off between the number of allocated subcarriers and the RIS size required to meet performance targets while also highlighting the influence of the transmitter MIMO array on link quality. Additionally, the proposed PSO algorithm efficiently reduces the number of RIS elements required to establish an RIS-assisted link while preserving the desired achievable rate. Finally, incorporating the RIS configuration time into the analysis enhances handover timing accuracy, thus improving PHO decision-making.

REFERENCES

[1] E. G. Larsson and et al., "Massive MIMO for next-generation wireless systems," *IEEE Commun. Mag.*, vol. 52, no. 2, pp. 186–195, Feb. 2014.

[2] S. Kutty and D. Sen, "Beamforming for millimeter-wave communications: An inclusive survey," *IEEE Commun. Surv. Tutorials*, vol. 18, no. 2, pp. 949–973, 2015, second Quarter.

[3] J. He, H. Wymeersch, and M. Juntti, "Channel estimation for RIS-aided mmWave MIMO systems via atomic norm minimization," *IEEE Trans. Wireless Commun.*, vol. 20, no. 9, pp. 5786–5797, Sep. 2021.

[4] M. Alrabeiah and et al., "Vision aided URLLC communications: Proactive service identification and coexistence," in *Asilomar Conf. Signals, Syst., Comput.* Pacific Grove, CA, USA: IEEE, Nov. 2020, pp. 174–178.

[5] H. Okamoto and et al., "Machine-learning-based throughput estimation using images for mmWave communications," in *2017 IEEE 85th Veh. Tech. Conf. (VTC Spring)*. IEEE, June 2017, pp. 1–6.

[6] M. Al-Quraan and et al., "Intelligent beam blockage prediction for seamless connectivity in vision-aided next-generation wireless networks," *IEEE Trans. Netw. Serv. Manag.*, vol. 20, no. 2, pp. 1937–1948, Jun. 2022.

[7] L. Mohjazi and et al., "An outlook on the interplay of AI and software-defined metasurfaces: An overview of opportunities and limitations," *IEEE Veh. Technol. Mag.*, vol. 15, no. 4, pp. 62–73, Dec. 2020.

[8] A. Adnan and et al., "Performance evaluation of IRS-Assisted Intra-cell handover in vision-aided mmWave networks," in *2024 IEEE Wireless Comm. and Net. Confe. (WCNC)*. Dubai, United Arab Emirates: IEEE, Apr. 2024, pp. 1–6.

[9] S.-K. Chou and et al., "On the aperture efficiency of intelligent reflecting surfaces," *IEEE Wireless Commun. Lett.*, vol. 10, no. 3, pp. 599–603, Mar. 2021.

[10] J.-B. Gros and et al., "A reconfigurable intelligent surface at mmWave based on a binary phase tunable metasurface," *IEEE Open J. Commun. Soc.*, vol. 2, pp. 1055–1064, May 2021.

[11] C. Feng and et al., "Near-field modeling and performance analysis for extremely large-scale IRS communications," *IEEE Trans. Wireless Commun.*, vol. 23, no. 5, pp. 4976–4989, May 2024.

[12] Y. Lu and L. Dai, "Near-field channel estimation in mixed LoS/NLoS environments for extremely large-scale MIMO systems," *IEEE Trans. Commun.*, vol. 71, no. 6, pp. 3694–3707, Jun. 2023.

[13] M. Al-Quraan and et al., "Enhancing reliability in federated mmWave networks: A practical and scalable solution using Radar-Aided dynamic blockage recognition," *IEEE Trans. Mobile Comput.*, vol. 23, no. 10, pp. 10 146–10 160, Oct. 2024.

[14] M. Alrabeiah, A. Hredzak, and A. Alkhateeb, "Millimeter wave base stations with cameras: Vision-aided beam and blockage prediction," in *2020 IEEE 91st Vehic. Tech. Conf. (VTC2020-Spring)*. IEEE, May 2020, pp. 1–5.

[15] H. Okamoto and et al., "Machine-learning-based throughput estimation using images for mmWave communications," in *2017 IEEE 85th Vehicular Technology Conf. (VTC Spring)*, Jun. 2017, pp. 1–6.

[16] S. Ohta and et al., "Point cloud-based proactive link quality prediction for millimeter-wave communications," *IEEE Trans. on Machine Learning in Commun. and Networking*, vol. 1, pp. 258–276, Sept. 2023.

[17] U. Demirhan and A. Alkhateeb, "Radar aided proactive blockage prediction in real-world millimeter wave systems," in *ICC 2022-IEEE Int. Conf. on Commun.* IEEE, May 2022, pp. 4547–4552.

[18] T. Jiang and et al., "Learning to beamform for intelligent reflecting surface with implicit channel estimate," in *GLOBECOM 2020-IEEE Global Commun. Conf.* IEEE, Dec. 2020, pp. 1–6.

[19] C. Jia and et al., "Machine learning empowered beam management for intelligent reflecting surface assisted MmWave networks," *China Commun.*, vol. 17, no. 10, pp. 100–114, Oct. 2020.

[20] C. You, B. Zheng, and R. Zhang, "Fast beam training for IRS-assisted multiuser communications," *IEEE Wireless Commun. Lett.*, vol. 9, no. 11, pp. 1845–1849, Nov. 2020.

[21] D. Ding and et al., "Environment-aware beam selection for IRS-aided communication with channel knowledge map," in *Proc. IEEE Globecom Wkshps (GC Wkshps)*. IEEE, Dec. 2021, pp. 1–6.

[22] G. C. Alexandropoulos and et al., "RIS-enabled smart wireless environments: Deployment scenarios, network architecture, bandwidth and area of influence," *EURASIP J. Wireless Commun. Netw.*, vol. 2023, no. 1, p. 103, Jan. 2023.

[23] M. Rossanese and et al., "Designing, building, and characterizing RF switch-based reconfigurable intelligent surfaces," in *Proc. 16th ACM Workshop Wireless Netw. Testbeds, Exp. Eval. & Char.*, Oct. 2022, pp. 69–76.

[24] X. Pei and et al., "RIS-aided wireless communications: Prototyping, adaptive beamforming, and indoor/outdoor field trials," *IEEE Trans. Commun.*, vol. 69, no. 12, pp. 8627–8640, Dec. 2021.

[25] J. Rains and et al., "High-resolution programmable scattering for wireless coverage enhancement: an indoor field trial campaign," *IEEE Trans. Antennas Propag.*, vol. 71, no. 1, pp. 518–530, Jan. 2022.

[26] Y. Liu and et al., "Reconfigurable intelligent surfaces: Principles and opportunities," *IEEE Commun. Surv. Tut.*, vol. 23, no. 3, pp. 1546–1577, May 2021.

[27] S. Hassouna and et al., "Indoor field trials for ris-aided wireless communications," in *2023 IEEE Int. Symp. Antennas Propag. USNC-URSI Radio Sci. Meet. (USNC-URSI)*. IEEE, Jul. 2023, pp. 75–76.

[28] M. Al-Quraan and et al., "Federated learning for reliable mmwave systems: Vision-aided dynamic blockages prediction," in *2023 IEEE Wireless Commun. Netw. Conf. (WCNC)*. Glasgow, UK: IEEE, Mar. 2023, pp. 1–6.

[29] M. Alrabeiah and et al., "ViWi: A deep learning dataset framework for vision-aided wireless communications," in *Proc. IEEE VTC-Spring*. IEEE, May 2020, pp. 1–5.

[30] E. Björnson and L. Sanguinetti, "Power scaling laws and near-field behaviors of massive MIMO and intelligent reflecting surfaces," *IEEE Open J. Commun. Soc.*, vol. 1, pp. 1306–1324, Sept. 2020.

[31] D. Dardari, "Communicating with large intelligent surfaces: Fundamental limits and models," *IEEE J. Sel. Areas Commun.*, vol. 38, no. 11, pp. 2526–2537, Nov. 2020.

[32] P. Wang and et al., "Fast beam training and alignment for IRS-assisted millimeter wave/terahertz systems," *IEEE Trans. Wireless Commun.*, vol. 21, no. 4, pp. 2710–2724, Apr. 2021.

[33] J. He and et al., "Learning to estimate RIS-aided mmwave channels," *IEEE Wireless Commun. Lett.*, vol. 11, no. 4, pp. 841–845, Apr. 2022.

[34] J. Perruisseau-Carrier and et al., "Contributions to the modeling and design of reconfigurable reflecting cells embedding discrete control elements," *IEEE Trans. Microw. Theory Techn.*, vol. 58, no. 6, pp. 1621–1628, Jun. 2010.

[35] M. Abualhayja'a and et al., "How much power is needed for RIS to beat relays? a sustainability framework," *TechRxiv*, Mar 2025.

[36] J. Rains and et al., "Reflecting metasurface unit cell design with multi-bit azimuthal control," in *Proc. Int. Conf. Microw., Antennas & Circuits (ICMAC)*. Chengdu, China: IEEE, December 2021, pp. 1–4.

RIS-Assisted Proactive Handover in mmWave Networks

Alaa Adnan, *Graduate Student Member, IEEE,* Mohammad Al-Quraan, *Graduate Student Member, IEEE,* Ahmed Zoha, *Senior Member, IEEE,* M. Majid Butt, *Senior Member, IEEE,* Sami Muhaidat, *Senior Member, IEEE,* Muhammad Ali Imran, *Fellow, IEEE,* Marco Di Renzo, *Fellow, IEEE,* and Lina Mohjazi, *Senior Member, IEEE*

***Abstract*—Millimeter-wave (mmWave) networks are highly vulnerable to line-of-sight (LoS) blockages. Vision-aided wireless communications (VAWC) enable proactive handovers (PHO) to address blockages in advance, ensuring seamless connectivity. However, PHO becomes challenging in scenarios where a nearby base station (BS) is unavailable. In such cases, reconfigurable intelligent surfaces (RIS) can restore connectivity. For RIS-assisted mmWave links to be practically deployed for a PHO, the RIS configuration time must be considered to ensure timely PHO. This key challenge stems from the large number of RIS elements, which limits the deployment in time-sensitive applications. For practical deployment, the RIS-assisted link must achieve a trade-off between 1) reducing signal processing complexity and 2) maintaining link quality. This can be accomplished by optimizing the RIS-assisted PHO process through minimizing the number of RIS elements required to maintain connectivity and accounting for the handover timing constraints. This work proposes a novel RIS-assisted PHO approach to maintain seamless connectivity during a blockage event. We formulate an optimization problem using particle swarm optimization (PSO) to determine the optimal end-to-end RIS-assisted link configuration setup. The proposed PSO approach reduced the required number of RIS elements to establish a link by 15% without compromising the desired link rate improving the signal strength by 15 to 30 dBm in the blocked area. Moreover, RIS configuration time is integrated into the PHO framework, ensuring accurate timing.**

***Index Terms*—Reconfigurable Intelligent Surfaces, Multiple Input Multiple Output,Vision Aided Wireless Communications, Particles Swarm Optimization.**

I. INTRODUCTION

Millimeter-wave (mmWave) technology has emerged as a promising candidate for sixth-generation (6G) networks due to its ability to support higher transmission rates [1]. Beamforming is envisioned to play a key role in mmWave systems, providing spatial reuse and reducing interference [2]. However, in terms of reliability, beamforming-based mmWave connectivity mainly relies on directive line-of-sight (LoS) links due to channel sparsity, which limits the usefulness of multipath components [3]. This makes mmWave signals highly susceptible to blockages, causing severe signal degradation when a LoS beam is obstructed.

Vision-aided wireless communication (VAWC) frameworks are expected to play a crucial role in 6G networks by leveraging visual information of the wireless environment to enable key applications including optimal beam selection based on user location [4], throughput estimation for choosing the best base station (BS) to serve a user [5], and, most importantly, beam blockage prediction in mmWave networks [6]. Meanwhile, reconfigurable intelligent surfaces (RIS) have emerged as a promising technology for enhancing signal quality and mitigating LoS blockages as the RIS can steer the signal towards a desired location using RIS-assisted links [7].

In our previous work [8], we integrated these two concepts into a unified framework to enhance reliability and address the blockage issue. The findings revealed that to provide acceptable signal strength, the RIS-assisted link must utilize a large RIS array to improve the signal quality. The need for larger RISs is attributed to the nearly passive nature of the RIS and the fact that the effective aperture area of an RIS is typically smaller than its actual physical area, further increasing the demand for a larger RIS to enhance link performance. The work in [9] introduced a mathematical model that accounts for the aperture area efficiency and proposed a modified path loss model based on the effective RIS area. Notably, the model considered the far-field assumption and estimated the RIS diameter to be approximately 20mm for a frequency of 28GHz, with an even smaller effective RIS area available for establishing a link. As a result, at higher frequency bands, the RIS effective area becomes even smaller. To overcome this limitation, achieving better performance requires deploying physically larger RISs.

The need for physically larger RISs operating in the mmWave band necessitates denser RIS configurations composed of smaller elements, due to the shorter wavelengths at these frequencies. Since each RIS element typically has an area smaller or equal to half of a wavelength squared, this implies that a significant number of elements can be accommodated per unit area. For instance, the authors in [10] fabricated and tested an RIS in both near-field and far-field scenarios. The fabricated RIS had an area of $10\text{ cm} \times 10\text{ cm}$, operated at 28GHz, and contained 400 RIS elements within this relatively small space. Deploying dense RISs operating in the mmWave

A. Adnan, M. Al-Quraan, A. Zoha, M. A. Imran and L. Mohjazi, are with the James Watt School of Engineering, University of Glasgow, Glasgow, G12 8QQ, UK. (e-mails: A.Bibi.1@research.gla.ac.uk, {Mohammad.Alquraan, Ahmed.Zoha, Muhammad.Imran, Lina.Mohjazi}@glasgow.ac.uk).

M. Majid Butt is with with Nokia Standards, USA. (e-mail: Majid.Butt@nokia.com).

S. Muhaidat is with the KU 6G Research Center, Department of Computer and Communication Engineering, Khalifa University, Abu Dhabi 127788, UAE, and also with the Department of Systems and Computer Engineering, Carleton University, Ottawa, ON K1S 5B6, Canada. (e-mail: sami.muhaidat@ku.ac.ae).

M. Di Renzo is with Université Paris-Saclay, CNRS, CentraleSupélec, Laboratoire des Signaux et Systèmes, 3 Rue Joliot-Curie, 91192 Gif-sur-Yvette, France (e-mail:marco.di-renzo@universite-paris-saclay.fr), and with King's College London, Centre for Telecommunications Research Department of Engineering, WC2R 2LS London, UK. (e-mail:marco.di_renzo@kcl.ac.uk).

band introduces several challenges, such as complex channel modeling, extensive channel estimation, and complex beam training, limiting the RIS application in real-time or time-sensitive applications.

The complexity of channel modeling arises from the fact that dense RISs necessitate near-field channel modeling. Assuming a fixed inter-element spacing equal to half a wavelength, the physical size of the RIS which determines the Fresnel distance is directly tied to the number of elements. With such a large number of RIS elements, satisfying far-field conditions often requires distances that exceed the Fraunhofer distance. This condition may result in a scenario where the link between the BS and the RIS operates in the far-field region, while the link between the RIS and the user remains in the near-field region [11].

Channel estimation in mmWave systems leveraging a large RIS with a high number of RIS elements presents a significant challenge. For instance, the study in [12] introduced an algorithm for channel estimation in near-field large-scale MIMO arrays, where the algorithm's complexity for non-line-of-sight (NLoS) paths depended on the number of scatterers required to reconstruct the signal. In the context of RIS channel estimation, near-field complexity is directly influenced by the number of RIS elements. In the next section, we will present the related work for beam blockage management in mmWave networks as an alternative to the explicit channel estimation approach and highlight the effect of the increased number of RIS elements on the system performance.

A. Related Work

In this section, we present state-of-the-art research that proposes solutions to beam blockages in high-frequency bands. The reviewed studies focus on beam blockage prediction and beam blockage mitigation by RIS-assisted links as an alternative to a blocked LoS.

1) Beam Blockage Prediction: Beam blockage prediction plays a crucial role in ensuring reliable communication, as it triggers the handover process to a link with better conditions than the blocked one. Two primary approaches are considered for predicting blockages: wireless information-based approaches and sensing information-based approaches [13]. Our focus will be on the sensing-based approach since it is the approach we are proposing in this work.

For sensing-based approach, various data acquisition techniques are employed for link blockage prediction, including VAWC frameworks, light detection and ranging (LiDAR) sensing, and radar-based blockage prediction. For instance, the work in [14] leveraged a VAWC framework, using a set of RGB images with predefined beamforming vectors to train a deep learning (DL) model for blockage prediction in mmWave networks. The work in [15] proposed the use of RGB images with depth cameras to train a machine learning (ML) model called adaptive regulation of wave vectors (AROW), facilitating proactive BS selection in blockage scenarios. The selection criterion was based on throughput estimations to ensure the best link for a handover. Additionally, [16] utilized LiDAR to acquire point cloud data for mmWave link quality prediction, forecasting radio propagation fluctuations caused by pedestrian obstructions. The work in [17] demonstrated that integrating radar-based sensing with mmWave BSs provides valuable information, such as velocity and range, which can aid in predicting network obstacles.

2) Beam Blockage Mitigation by RIS-Assisted Links: RIS-assisted links provide an effective solution for replacing blocked LoS links by redirecting incident signals to obstructed users. The potential to reduce channel estimation and beam training overhead has garnered significant interest in enhancing the practical deployment of RISs, particularly for time-critical or real-time applications.

The study in [18] aimed to optimize RIS performance by jointly designing BS beamforming and RIS reflection coefficients. The proposed approach maximized the user's sum rate by directly optimizing received pilots at the BS using a graphical neural network (GNN) learning model. This method eliminated the need for explicit channel estimation. Results demonstrated that incorporating additional information, such as user location reduced pilot transmission achieving optimal beamforming and RIS reflection settings. Despite these improvements, the complexity of the beamforming matrix design remains directly proportional to the number of RIS elements, leading to increased training delays. This led the authors to assume that GNN training is performed offline to mitigate the impact of runtime delays in online scenarios.

Another promising approach involves intelligent RIS beam management (BM) and beam training (BT) instead of explicitly estimating channel state information (CSI). For example, [19] trained a ML model within a BM framework to process environmental and user mobility data, enhancing BM in beam blockage scenarios. The work in [20] employed BT to estimate the best beam selection for the receiver. However, this method heavily depended on RIS phase shifter resolution, often assuming an ideal continuous phase shifter capable of selecting the optimal beam with minimal directivity loss.

Furthermore, [21] proposed a joint active and passive beamforming design for optimal beam selection in RIS-assisted networks, utilizing the concept of a channel knowledge map (CKM). This approach builds a site database that correlates beams with users' geographical locations, aiding in optimized beam selection. Also, this work highlighted the fact that BT overhead is directly related to the number of RIS elements, and with the large number of mmWave RIS elements, BT will be a challenging task.

Despite advancements in beam blockage prediction and mitigation techniques, integrating an RIS with a VAWC framework for a seamless RIS-assisted handover has not been explored in prior studies as the authors assumed the availability of a BS to which the blocked user can be handed over. However, in some scenarios, a second BS may not be available. Additionally, most RIS-related works assume that user locations and blockage information are either known at the BS or rely on probabilistic models, which are unsuitable for dynamic real-time scenarios. Another overlooked factor is the impact of RIS configuration time on system performance.

Moreover, even with BM and BT techniques, mmWave RIS implementations still require a large number of RIS elements

for acceptable performance. In our previous study [8] we performed a system performance analysis for a mmWave RIS-assisted link operating at 60GHz, the findings indicated that at least 1000 RIS elements are necessary to establish a link with sufficient signal strength, making signal processing a highly complex task and increasing BT overhead. Therefore, optimizing the RIS-assisted handover process by minimizing the required number of RIS elements while maintaining link quality is crucial for practical deployment.

B. Motivation and contribution

The aforementioned research studies indicate that realizing RIS-assisted mmWave communication requires a significantly large number of RIS elements. This work aims to leverage an RIS-assisted link in a proactive handover (PHO) process to replace a blocked LoS connection. However, deploying large-scale mmWave RIS-assisted communication systems presents several challenges, which become critical bottlenecks for time-sensitive applications such as PHO, as they are constrained by narrow time windows for triggering the handover process.

To effectively leverage RIS for PHO, two key deployment challenges must be addressed:

- Ensure that the RIS has a sufficient number of elements to maintain the required link quality.
- Ensure that the time needed to configure the phase shifts of the RIS elements is within the acceptable time limit to trigger handover before the occurrence of a blocking event.

From a practical deployment perspective, finding a trade-off between achieving the desired RIS-assisted link quality and mitigating signal processing complexity, particularly in channel estimation and modeling, is crucial. This trade-off can be realized by efficiently minimizing the number of RIS elements while maintaining acceptable link quality, such as a target achievable rate. Such an approach not only reduces the complexity of channel estimation and BT overhead but also enhances the feasibility of RIS-assisted links for real-time applications. Since PHO depends on accurate timing to trigger the process, the time required for RIS configuration becomes a critical factor in ensuring a successful PHO. However, no studies have specifically focused on the impact of RIS configuration time on PHO timing. In the surveyed literature, RIS configuration time was either estimated or assumed for purposes unrelated to PHO considerations.

The work presented in [22] suggested that RIS configuration response times need to fall within a granular range of 20 to 100 milliseconds (ms) to support effective communications. The study in [23] employed the STM32L071V8T6 microcontroller unit to control RIS phase shift configurations, reporting a configuration time of less than 35 ms. Meanwhile, the work in [10] utilized a field-programmable gate array (FPGA) for RIS phase shift control, where the configuration delay ranged from 0.22 ms to 7 ms, depending on the number of RIS elements. These measurements also used to indicate wiring complexity in RIS fabrication, highlighting the challenges of managing more mmWave RIS elements, including greater fabrication difficulty, control complexity, and longer configuration time.

In these studies, the RIS configuration time was not considered within the context of a communication framework such as PHO. A deeper understanding of the factors influencing RIS configuration time is essential for the effective and practical deployment of RIS-assisted links in time-critical operations such as handovers and user tracking. To the best of the authors' knowledge, no prior work has addressed the impact of RIS configuration time on PHO in RIS-assisted links.

mmWave RIS-assisted systems are envisioned to play a significant role in 6G networks, enabling the realization of smart environments (SE) supporting applications such as road safety and autonomous vehicles in ultra dense networks (UDNs) all of which demand seamless and uninterrupted connectivity. However, considering the challenges outlined above, deploying RISs with a large number of elements introduces several issues that hinder the practical implementation of RIS-assisted links. Therefore, achieving a balance between RIS link quality and minimizing the RIS configuration time in which both are directly related to the number of RIS elements is crucial for enabling timely handover execution. Since the primary objective of this work is the effective deployment of RIS-assisted links to replace blocked mmWave LoS connection within a PHO framework, addressing these challenges is essential. In this context, the key contributions of this work can be summarized as follows:

- Integration of RIS-assisted mmWave connectivity within a novel VAWC framework to enable blockage prediction and precise user localization, thereby facilitating accurate beam steering from the RIS toward the blocked region.
- Proposing a novel RIS-assisted PHO framework that explicitly incorporates RIS configuration time into the PHO timing process, ensuring accurate triggering during LoS blockage scenarios.
- An optimization algorithm is proposed to enhance the responsiveness of the RIS-assisted PHO process by minimizing RIS configuration time, while maintaining the desired link quality.

The rest of this paper is organized as follows: In Section II, the system and channel models are presented. Section III discusses the problem formulation and optimization approach. Section IV introduces the proposed RIS-assited PHO framework. Section V provides the results and key findings. Finally, Section VI gives concluding remarks.

II. System and channel models

In this section, we provide a comprehensive description of the RIS architecture and configuration time estimation, which will be integrated into the VAWC PHO framework, along with the system and channel models.

A. RIS Configuration Time Estimation

In order to effectively deploy an RIS-assisted link in a PHO procedure, the RIS configuration time required to steer the signal toward a blocked area must be accounted for to ensure accurate triggering and seamless connectivity.

This work builds upon our previous study [8], which proposed a PHO framework (see Fig. 1) that leverages RIS-assisted beamforming in a blockage scenario (see Fig. 2). The RIS-assisted beam is selected from a pre-stored set of RIS beamforming configurations maintained in a CKM database. However, the PHO framework in [8] did not account for RIS configuration time as part of the PHO timing scheme, which is a critical factor for ensuring accurate PHO execution.

The framework proposed in [8] was based on the original PHO framework introduced in [6], which utilized VAWC and RGB cameras powered by the You Only Look Once version 3 (YOLOv3) object detection algorithm to detect blockages. The detected blockage data was then used to train a neural network (NN), which relied on user mobility speed to determine the optimal triggering point for the PHO process. However, the framework in [6] did not consider PHOs involving an RIS. Instead, it proposed performing a PHO to a secondary BS when a blockage occurs. In practice, a secondary BS may not always be available as explained in section I, making an RIS-assisted link a promising and practical alternative for handover and, thus, worth further investigation.

In the original framework proposed by [6], two important timing factors were estimated: the execution time T_{exec} and the waiting time T_{W} before triggering the handover. T_{exec} is defined as the time required for the proposed algorithm to be completed, starting when the images are captured by the BS and processed for blockage detection until the PHO process is completed. The value of T_{W} is given as follows [6]

$$T_W = T_{\text{to-BLK}} - T_{\text{exec}} \ , \tag{1}$$

where $T_{\text{to-BLK}}$ represents the time for a user to encounter a blockage. T_W varies based on the user's location and movement speed. Selecting the value of T_W is critical for defining the optimal PHO trigger region, allowing the algorithm to determine the best time to perform the PHO.

In order to integrate the RIS as part of the PHO framework T_{exec} must include T_c the RIS response time represented by the required configuration time to steer the signal to a blocked user. As a result, the updated execution time, denoted as $T_{\text{exec}}^{\text{RIS}}$, can be expressed as

$$T_{\text{exec}}^{\text{RIS}} = T_{\text{exec}} + T_{\text{c}} \ , \tag{2}$$

This leads to a new waiting time, $T_{\text{W}}^{\text{RIS}}$, which is given by

$$T_{\text{W}}^{\text{RIS}} = T_{\text{to-BLK}} - T_{\text{exec}}^{\text{RIS}} \ , \tag{3}$$

The new $T_{\text{W}}^{\text{RIS}}$ now includes the RIS configuration time T_c, in order to be able to estimate T_c we examine the RIS architecture and identify the factors contributing to the configuration time.

The design approach for RIS can vary based on multiple factors, such as indoor or outdoor deployment, operating frequency, RIS element design, and several other considerations. This work does not focus on the specific details of the radio frequency design aspects of RIS. Instead, it emphasizes the control layer setup and its impact on the configuration time.

The RIS consists of three main layers, as shown in Fig. 3: the front layer, which is a grid of RIS elements; the RIS back-layer board; and the control layer. The front layer of the RIS board typically consists of N RIS elements, each embedded with B diodes to control the phase shift of the incident signal for beam steering. The most commonly deployed diodes include varactor diodes [24] and PIN diodes [25].

The control layer is responsible for transmitting configuration bits to the RIS back-layer board. The back layer of the RIS board houses a set of logic circuits that control the diodes embedded in each RIS element, enabling them to switch on or off as needed [26]. This layer typically contains multiple shift registers, where the number of registers is generally $\leq N$, depending on the number of diodes embedded in each element and the shift register bus capacity. Since each diode requires one bit to be switched on or off, the shift registers are used by the controller layer to push the configuration bits via serial-to-parallel transmission, efficiently controlling the diode states. Different setups of shift registers controlling the RIS elements are presented in [10], [25], and [27].

The configuration time required for the RIS depends on several factors, including the transmission rate of the control board, the clocking rate of the shift registers, the number of RIS elements, and the number of diodes embedded within each element [10]. Thus, the codeword, representing the total number of bits required to configure the RIS, is determined by multiplying the total number of RIS elements by the number of diodes in each element. Each bit is used to switch a single diode on or off, enabling the desired beamforming setup of the RIS. When configuring the RIS remotely from the server, the interface speed directly impacts the configuration time. However, if the configuration states are stored locally in the microcontroller layer and the required codeword is directly pushed to the shift registers, the configuration time depends primarily on the clocking rate of the shift registers [10]. The work in this paper adopts the latter concept, and accordingly, the required time for RIS configuration is expressed as

$$T_c = \frac{NB}{C_{lk}} \ , \tag{4}$$

where C_{lk} represents the clocking rate of the shift registers.

From equation (4), along with the additional delays accounted for in equation (3), it can be deduced that reducing signal processing complexity and BT overhead while ensuring a faster RIS configuration response requires minimizing N without compromising link quality. By identifying the optimal value of N, we can estimate the RIS configuration time. As described in equation (4), N is a key factor in estimating T_c, since both B and Clk are fixed for each element and the shift register. This optimization approach will be further explored in Section III, where the proposed algorithm to achieve this goal will be introduced.

B. System Model

We consider a BS operating in the mmWave band, assisted by an RIS, where the BS transmits to a single-antenna user. The BS coverage area is served by multiple uniform linear array (ULA) sectors, with each ULA responsible for a specific segment of the coverage area. Each ULA sector comprises M antenna elements. To monitor the environment, the BS

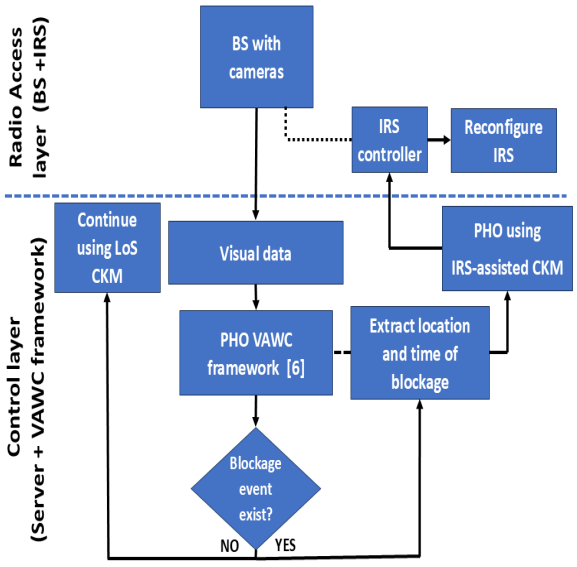

Figure 1: RIS-assisted PHO framework [8].

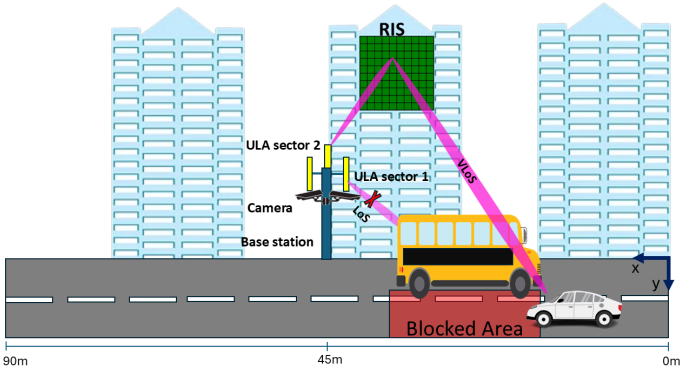

Figure 2: RIS-assisted vision-aided BS setup.

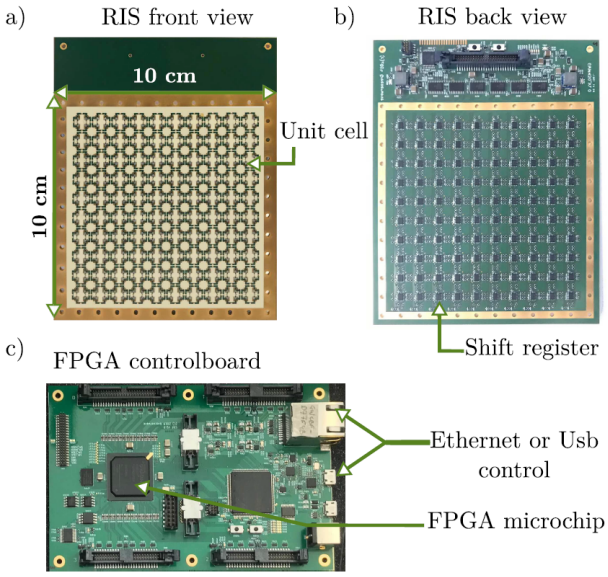

Figure 3: RIS controller board: (a) front layer of RIS elements grid, (b) back layer of shift registers grid, and (c) RIS controller board [10].

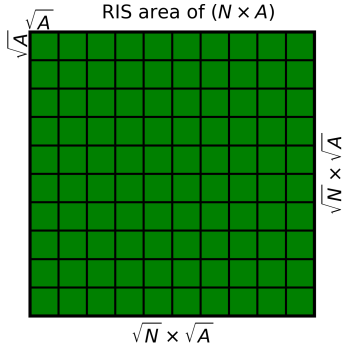

Figure 4: RIS area equals to $N \times A$.

is equipped with a set of cameras that oversee the street, as illustrated in Fig. 2. These cameras are used to determine the user's location and detect potential blockages [28].

The system employs orthogonal frequency-division multiplexing (OFDM) with K subcarriers as the resource allocation scheme for radio access. The mmWave BS system utilizes an analog beamforming technique, where the user is served by a beam represented by a beamforming vector selected from a predefined codebook $\mathcal{F} = \{f_i\}_{i=1}^{B_m}$, where $\mathbf{f}_i \in \mathbb{C}^{M\times 1}$ and B_m represents the total number of beams. Each beam, denoted as $\mathbf{f}_i$, can be expressed as follows

$$\mathbf{f}_i = \frac{1}{\sqrt{M}} \begin{bmatrix} 1 & e^{j2\pi \frac{d}{\lambda} \sin\theta_i} & \dots & e^{j2\pi \frac{d}{\lambda}(M-1)\sin\theta_i} \end{bmatrix}^T, \quad (5)$$

where $j = \sqrt{-1}$, T represents the transpose operation of a vector, d is the antenna element spacing, λ is the wavelength of the transmitter, and $\theta_i \in \left\{ \frac{2\pi i}{B_m} \right\}_{i=0}^{B_m-1}$ denotes the steering angle from the BS towards the desired user.

This study adopts the blockage scenario from the original dataset [29], where co-located cameras detect a bus obstructing the LoS signal to the served user. We extend the system setup by introducing an RIS, as illustrated in Fig. 2, to address anticipated beam blockages within the VAWC framework proposed in [6]. Instead of performing a handover to a secondary BS, as suggested in [6], this work proposes establishing a virtual line-of-sight (VLoS) link using the RIS. This VLoS link is leveraged by the PHO procedure as an alternative to the obstructed LoS link.

The RIS is comprised of elements, each of an area given by $A = \left(\frac{\lambda}{2}\right)^2$. The dimensions of each element are $(\sqrt{A} \times \sqrt{A})$, the elements are arranged in a planar square grid of size $(\sqrt{N} \times \sqrt{A})$. The total area of the RIS is $(N \times A)$ [30] as illustrated in Fig. 4. We assume the RIS is mounted on the facade of a building located behind the BS at a sufficient height to overcome obstructions. The RIS can dynamically steer the beam using a predefined $N \times N$ codebook, denoted by $\mathcal{V}$, comprised of steering coefficients expressed as

$$v_{mn} = \alpha e^{j\frac{2\pi d_{\text{RIS}}}{\lambda}\sin\theta_{mn}}, \quad (6)$$

where $v_{mn} \in \mathbb{C}^{N\times N}$, α is the reflection coefficient of each RIS element, and $m, n = 1, \dots, N$. Additionally, d_{RIS}

represents the RIS element spacing, and $\theta_{mn} \in [0, 2\pi]$ denotes the RIS steering angle.

To facilitate the PHO, each ULA sector is equipped with a camera to capture visual information. This data is processed by the VAWC framework to extract critical parameters for predicting a blockage event in advance, such as the existence of a blocking object, the user's speed toward the blocked area, and the estimated time and location of the blockage. Based on this information, the VAWC framework enables the BS to steer the RIS beam toward the anticipated blockage area, leveraging the PHO framework illustrated in Fig. 1 to define the optimal time for triggering the PHO.

C. LoS Channel Model

The user transmits a pilot signal, which is used to train the beam set B_m and select the optimal beam that maximizes the signal-to-noise ratio (SNR). This work adopts the pilot signal/beam training methodology described in [13]. Once the optimal beam is identified, it is utilized for downlink communication. The baseband mmWave signal transmitted from the BS to the user over a LoS link, in the absence of a blockage, is expressed as

$$y_{\text{los},k} = \mathbf{G}_{\text{los},k}\mathbf{f}^{\star}_{\text{los},k}s_{\text{los},k} + n_{\text{los},k} \ , \tag{7}$$

where, $s_{\text{los},k}$ represents a transmitted symbol, $n_{\text{los},k} \sim \mathcal{CN}(0, \sigma^2)$ represents the additive white gaussian noise (AWGN) for the k-th subcarrier with zero mean and variance of σ^2, $\mathbf{G}_{\text{los},k}$ is the channel gain which is expressed as [6]

$$\mathbf{G}_{\text{los},k} = \sqrt{\beta_k}\,(\mathbf{h}_k)^T e^{\left(j2\pi\frac{kd}{K\lambda}\right)} f(\theta,\phi)_k \ , \tag{8}$$

In equation (8), β_k represents the large-scale fading coefficient, $f(\theta,\phi)_k$ is the function of the angles of departure and arrival, respectively, where θ is the azimuth angle and ϕ is the elevation angle. $h_k \in \mathbb{C}^{M\times K}$ is the small-scale fading channel coefficient.

Since the objective of this work is to minimize the number of RIS elements, i.e., the overall RIS area, to reduce configuration time, the channel gains must account for both the transmitter and RIS areas as functions of the number of antenna elements. Thus, β_k is modeled as a function of the transmitter and receiver antenna areas, as described in [31]

$$\beta_k = \frac{A_t A_U}{(\lambda d_{BU})^2} \ , \tag{9}$$

where A_t is the transmitter antenna arrea, A_t can be expressed as $A_t = M \times A_{\text{MIMO}}$, where A_{MIMO} denotes the area of a single antenna element. Similarly, A_U corresponds to the area of a single receiver antenna element. In this work both A_{MIMO} and A_U are set to have an area of $\left(\frac{\lambda}{2}\right)^2$. Additionally, d_{BU} is the distance between the BS and the user.

The optimal beam, selected to establish the best link to the user at a given location, is determined as follows [6]

$$\mathbf{f}^{\star}_{\text{los},k} = \underset{\mathbf{f}\in\mathbf{F}}{\text{argmax}} \frac{1}{K}\sum_{k=1}^{K}\log_2\left(1+\rho\left|\mathbf{G}_{\text{los},k}\mathbf{f}\right|^2\right) \ , \tag{10}$$

where ρ represents the power-to-noise ratio, defined as $\frac{P_t}{\sigma^2}$ with P_t being the transmitted power. Based on this equation, the achievable rate R is evaluated as follows [29]

$$\text{R}_{\text{los}} = \frac{1}{K}\sum_{k=1}^{K}\log_2\left(1+\rho\left|\mathbf{G}_{\text{los},k}\mathbf{f}^{\star}_{\text{los},k}\right|^2\right) \ . \tag{11}$$

D. VLoS Channel Model

Whenever a blockage event is detected by the VAWC framework, an RIS-assisted link is utilized to perform a PHO [8]. The signal received through the RIS beam can be expressed as

$$y_{\text{VLoS}} = (\mathbf{v}^{\star})^H \mathbf{G}_{\text{VLoS}}\mathbf{f}^{\star}_{\text{BI}}s_{\text{VLoS}} + n_{\text{VLoS}} \ , \tag{12}$$

where, s_{VLoS} reresents the transmitted symbol through the VLoS link, $(\mathbf{v}^{\star})^H\mathbf{G}_{\text{VLoS}}\mathbf{f}^{\star}_{\text{BI}}$ denotes the total cascaded end-to-end channel from the BS to the blocked user through the RIS, $\mathbf{f}^{\star}_{\text{BI}}$ represents the optimal beam from the BS to the RIS, and $\mathbf{v}^{\star}$ denotes the optimal RIS steering vector that maximizes R. Additionally, H refers to the Hermitian transpose operation [21] [32].

In order to capture a practical system performance we adopt the scenario mentioned earlier in section I where the link from the BS to RIS falls in the far-field model and the link from the RIS to the user falls in the near-field model thus $\mathbf{G}_{\text{VLoS}}$ is comprised of two channel gains. The first characterizes the link from the BS to the RIS and is expressed by the far-filed model similar to the equation (9) as follows

$$\beta_{BI} = \frac{A_t A_{\text{RIS}}}{(\lambda d_{BI})^2} \ , \tag{13}$$

A_{RIS} is the RIS area and is expressed as $A_{\text{RIS}} = N \times A$, where A represents the area of a single RIS element, and d_{BI} is the distance between the BS and the RIS [30].
For the second part of the cascaded channel, specifically the link from the RIS to the blocked user, the channel is assumed to be in the near-field model and can be expressed as [31]

$$\beta_{IU} = \frac{4A_{\text{RIS}}}{3\lambda^2}\left(\frac{\sqrt{2\left(\frac{(d_{IU})^2}{A_U}\right)}}{\sqrt{1+2\left(\frac{(d_{IU})^2}{A_U}\right)}\left(1+4\left(\frac{(d_{IU})^2}{A_U}\right)\right)} + 2\cot^{-1}\left(\sqrt{8\left(\frac{(d_{IU})^2}{A_U}\right)\left(1+2\frac{(d_{IU})^2}{A_U}\right)}\right)\right) \ , \tag{14}$$

here, d_{IU} represents the distance from the RIS to the blocked user. Therefore, the final channel coefficients of the cascaded channel G_{VLoS} can be expressed as

$$\mathbf{G}_{\text{VLoS,k}} = \sqrt{\beta_{IU}\beta_{BI}}\mathbf{h}_{c,k}e^{\left(j2\pi\frac{k(d_{\text{RIS}}+d_{\text{MIMO}})}{K\lambda}\right)}f(\theta,\phi), \tag{15}$$

where $\mathbf{h}_{c,k}$ is the small-scale fading coefficient for the cascaded channel. In our work, we assume perfect CSI however, our primary focus is on capturing the impact of large-scale fading in the near-field, where path loss becomes the dominant factor influencing the required number of RIS elements. Instead of employing high-resolution angle-dependent beamforming for near-field modeling which introduces substantial computational complexity we focus on large-scale fading. This

Symbol	Definition
M	Number of ULA MIMO elements
N	Number of IRS elements
f , v	BS, IRS predefined beams vectors
K	Number of OFDM subcarriers
P_t	Transmitted power
ρ	Power-to-noise ratio
λ	Carrier wavelength
G	Channel gain parameter
β , h	Large and small scale fading parameters
$f(\theta, \phi)$,	Function of angles of arrival and departure
θ , ϕ	Azimuth and elevation angles
A_T	MIMO ULA array area
A_{RIS}	RIS grid area
A	RIS element area
A_{MIMO}, A_U	Antenna element area for MIMO and user
d	Antenna element spacing
d_{BI}	Distance from BS to RIS
d_{IU}	Distance from RIS to user
R	Achievable rate
B	Number of didoes per RIS elements
C_{lk}	Shift register clocking rate
T_c	RIS configuration time
T_W^{RIS}	Waiting time before triggering PHO

Table I: Key notation used in system and channel models.

choice is motivated by the fact that computational complexity is directly related to the codebook size, as discussed in the computational complexity section of the paper. The achievable rate of the RIS VLoS link can be expressed as

$$\mathrm{R}_{\mathrm{VLoS}} = \frac{1}{K}\sum_{k=1}^{K}\log_2\left(1+\rho\cdot\left|(\mathbf{v}^{\star})^H\mathbf{G}_{\mathrm{VLoS},k}\mathbf{f}_{\mathrm{BI}}^{\star}\right|^2\right). \quad (16)$$

III. Problem formulation and suggested optimization

The main objective of this work is to minimize the number of RIS elements N, and subsequently the RIS configuration time T_c, in order to reduce the signal processing complexity BT overhead, while maintaining the desired achievable rate. Striking a balance between minimizing N and preserving the required link performance is essential to ensure efficient and timely execution of the PHO process. This trade-off is particularly critical for enabling RIS-assisted links to support time-sensitive applications, such as autonomous driving and real-time user tracking.

A. Problem Formulation

The purpose of the optimization process presented in this work is to determine the optimal configuration for the end-to-end RIS-assisted system, taking into account key parameters such as the number of dedicated subcarriers K, the transmitter specifications represented by the number of antenna elements M, the transmission power, and the selection of optimal beamforming vectors from the BS to the RIS and from the RIS to the blocked user.

This study investigates the optimization of the number of RIS elements under two distinct scenarios. In the first scenario, the RIS is assumed to be equipped with ideal continuous phase shifters, enabling highly accurate beam steering with minimal directivity losses. This idealized model offers reduced computational complexity and serves as a theoretical benchmark. In contrast, the second scenario considers a more practical deployment in which the RIS employs discrete phase shifters. In this case, the configuration is influenced by the number of diodes per RIS elelemnt B, which governs both the number of available RIS beamforming patterns and the number of bits required to configure the RIS. Although this scenario introduces increased computational overhead, it reflects real-world hardware limitations more accurately. These two scenarios collectively provide insights into the trade-off between computational complexity and practical feasibility in RIS-assisted mmWave systems. Based on that, the optimization problem is formulated for each scenario as follows.

*1) **Scenario 1**:* The RIS has an ideal continuous phase shifter. By substituting equations (13), (14), and (15) into equation (16), the achievable rate can be expressed as

$$\mathrm{R}_{\mathrm{VLoS}} = \frac{1}{K}\sum_{k=1}^{K}\log_2\left(1+\rho MN^2C\left|\mathbf{h}_{c,k}\mathbf{f}_{\mathrm{BI}}^{\star}\right|^2\right), \quad (17)$$

where the beam $\mathbf{f}_{\mathrm{BI}}^{\star}$ is selected to maximize the RIS link SNR for the blocked user [6]

$$f_{\mathrm{BI}}^{\star} = \underset{f_{\mathrm{BI}}\in\mathcal{F}}{\operatorname{argmax}}\frac{1}{K}\sum_{k=1}^{K}\log_2\left(1+MN^2C\rho\left|h_{c,k}f_{\mathrm{BI}}\right|^2\right), \quad (18)$$

where

$$C = \frac{4A^2A_{\mathrm{MIMO}}}{3\lambda^4d_{\mathrm{BI}}^2}\left(\frac{\sqrt{2Q}}{\sqrt{1+2Q}\,(1+4Q)} + 2\cot^{-1}\left(\sqrt{8Q\,(1+2Q)}\right)\right) \times e^{j2\pi\frac{k(d_{\mathrm{RIS}}+d_{\mathrm{MIMO}})}{K\lambda}}, \quad (19)$$

where $Q = \frac{d_{\mathrm{IU}}^2}{A_U}$. As part of the continuous phase shifter assumption, the RIS beamforming vector $\mathbf{v}^{\star}$ is assumed to effectively counteract the values generated by $f(\theta,\phi)$ in equation (15). Through mathematical manipulation of equation (17) a function in terms of N can be found as

$$N = \left(\frac{2^{RK}}{\prod_{k=1}^{K}MC\rho\left|h_{c,k}f_{\mathrm{BI}}^{\star}\right|^2}\right)^{\frac{1}{2K}}, \quad (20)$$

and subsituting (20) in equation (4) the objecctive function to minimize T_c can be expressed as follows:

$$(\mathrm{P1}): \quad \min_{M,K,f_{\mathrm{BI}}^{\star}} \quad T_c = \frac{B}{C_{lk}}\left(\frac{2^{RK}}{\prod_{k=1}^{K}MC\rho\left|h_{c,k}f_{\mathrm{BI}}^{\star}\right|^2}\right)^{\frac{1}{2K}} \quad (21)$$

subject to:

$$R \geq R_{\mathrm{th}}, \quad (21.a)$$

$$M_{\min} \leq M \leq M_{\max}, \quad (21.b)$$

$$P_{\min} \leq P_t \leq P_{\text{budget}}, \tag{21.c}$$
$$1 \leq K \leq K_{\max}, \tag{21.d}$$

*2) **Scenario 2**:* The RIS is equipped with a discrete phase shift, where the number of available beams is dependent on B

$$\mathbf{v} = \text{DFT}(2^B)\ , \tag{22}$$

where $\text{DFT}(2^B)$ refers to the discrete Fourier transform function for RIS beamforming. In this case, the achievable rate can be expressed as

$$\text{R}_{\text{VLoS}} = \frac{1}{K}\sum_{k=1}^{K}\log_2\left(1+\rho MN^2C\left|(\mathbf{v}^\star)^H\mathbf{h}_{c,k}\mathbf{f}_{\text{BI}}^\star\right|^2\right)\ , \tag{23}$$

where the pair of beams $\mathbf{f}_{\text{BI}}^\star$ and $\mathbf{v}^\star$ are selected to maximize the RIS link SNR for the blocked user [21] [32]

$$(\mathbf{v}^\star, \mathbf{f}_{\text{BI}}^\star) = \underset{\mathbf{f}\in\mathcal{F},\mathbf{v}\in\mathcal{V}}{\text{argmax}}\frac{1}{K}\sum_{k=1}^{K}\log_2\left(1+\rho\left|(\Omega^T\otimes\mathbf{f}_{\text{BI}})\mathbf{G}_{\text{VLoS},k}\right|^2\right)\ , \tag{24}$$

where $\Omega = \text{diag}(\mathbf{v})$, and $\otimes$ denotes the Kronecker product operation [33], hence the objective function for T_c can be determined from equations (4) and (23) as follwos

$$\text{(P2)}: \min_{M,K,f_{\text{BI}}^\star,v^\star} \quad T_c = \frac{B}{C_{lk}}\left(\frac{2^{RK}}{\prod_{k=1}^{K}MC\rho\left|(v^\star)^H h_{c,k}f_{\text{BI}}^\star\right|^2}\right)^{\frac{1}{2K}} \tag{25}$$

subject to:

$$R \geq R_{\text{th}}, \tag{25.a}$$
$$M_{\min} \leq M \leq M_{\max}, \tag{25.b}$$
$$P_{\min} \leq P_t \leq P_{\text{budget}}, \tag{25.c}$$
$$1 \leq K \leq K_{\max}. \tag{25.d}$$

It is worth mentioning that equations (18) and (24) in both scenarios do not represent constraints, but rather internal beam selection rules that must be employed to maximize the SNR during the evaluation of the objective function. The optimal beams $\mathbf{f}_{\text{BI}}^\star$ and $\mathbf{v}^\star$, selected through this process, directly influence the achievable rate and thereby contribute to minimizing the number of RIS elements required to establish a reliable link. Thus, in each iteration of the optimization process, the selection of the optimal beams follows the steps outlined in (Algorithm 1). The process begins by setting the transmitter and RIS specifications, followed by the calculation of the optimal beams. Further details of the optimization approach are provided in the following section.

The objective function and its associated constraints are designed to minimize the configuration time for establishing an RIS-assisted link by indirectly reducing the required number of RIS elements needed to achieve a target data rate. This is accomplished by selecting the optimal combination of transmitter MIMO antenna size, allocated OFDM subcarriers, and RIS beamforming vectors to maximize the effective SNR across all subcarriers. The constraints enforce practical limitations, such as meeting minimum data rate requirements, respecting hardware and power limitations, and selecting beams from discrete codebooks that best align with the propagation environment.

Algorithm 1 Selecting optimal BS & RIS beams to minimize T_c

1: **Input:** MIMO transmitter antenna range $M_{\min}, M_{\max}$, RIS resolution B, and other system parameters
2: **for** each iteration **do**
3: Set transmitter antennas M
4: Compute BS MIMO beamforming codebook size: $\mathcal{F}$
5: Compute RIS beamforming codebook size: $\mathcal{V}$
6: Calculate optimal beam $f_{\text{BI}}^\star$ using equation (18)
7: Calculate optimal RIS beam $v^\star$ using equation (24)
8: Evaluate T_c using the objective functions in (21) or (25) based on the considered scenario
9: **end for**
10: **Output:** Optimal configuration $\mathbf{f}_{\text{BI}}^\star$ and $\mathbf{v}^\star$ for minimizing T_c

The optimization problems formulated in equations (21) and (25) are both non-convex because of variables such as K and $f_{\text{BI}}^\star$ are discrete in nature, while others like ρ can be considered continuous, resulting in a mixed-variable domain. Also, the beam selection functions presented in (18) and (24) are both non-convex. These properties render traditional gradient-based or convex solvers unsuitable for this scenario.

B. Proposed optimization algorithm

This work is the first to explore the concept of environment-aware RIS-assisted PHO, establishing a foundational baseline for future research directions such as proactive user tracking to address the limitations associated with the passive nature of RIS technology. The optimization is performed in an offline approach to construct a site-specific CKM, thereby ensuring that the algorithm's convergence time does not impact real-time system responsiveness. The CKM enables a fast RIS configuration setup selection to steer the signal toward the predicted blockage location in online scenarios. This approach enables efficient and timely handover execution. Future research may involve periodic updates to the CKM using ML prediction techniques and digital twin models to further enhance accuracy in highly dynamic mmWave environments.

Metaheuristic optimization methods have become a natural choice for effectively handling non-convexity and mixed-variable system models. These algorithms do not rely on gradient information and can explore large and complex solution spaces for suboptimal solutions. Among various metaheuristic methods such as genetic algorithms (GA), simulated annealing (SA), and ant colony optimization (ACO), Particle Swarm Optimization (PSO) stands out as particularly well-suited for this problem.

PSO offers several advantages in this context. It is simple to implement, requiring fewer hyperparameters than GA or SA, and due to this fact it exhibits faster convergence time per iteration. Moreover, PSO leverages swarm intelligence by balancing individual particle exploration and global exploitation, which improves the search for the best suboptimal solution.

PSO is an effective optimization algorithm widely employed for solving complex problems involving multiple parameters and of a discrete nature. The use of PSO has been applied to optimize the states of the RIS elements for uniform phase change [34], [35], and to optimize the spacing of RIS elements [25] [36].

In this work, we propose the use of PSO to achieve the desired trade-off between minimizing the number of RIS elements while maintaining the desired link rate, leading to estimating the RIS configuration time T_c. The optimizer identifies the optimal parameters, such as K, P_t, M, and the optimal beams $\mathbf{v}^\star$ and $\mathbf{f}_{\text{BI}}^\star$ by following the steps outlined in (Algorithm 2) and the proposed algorithm is used to solve ($\mathbf{P1}$) and ($\mathbf{P2}$) depending on the scenarios considered.

The algorithm begins by setting the maximum number of iterations and the number of particles that will explore both the local and global solutions within the solution space of the parameters. The first step is to find the optimal transmitter specifications represented by M. At the start of each iteration, the algorithm initializes the population of particles at random positions to search in parallel across the entire solution space. The particles randomly select M, which represents the required number of ULA transmitter elements needed to establish a link with the desired R. The number of transmitter antenna elements M is selected from a range bounded by M_{min} and M_{max}. Within this range, M is discretized into fixed block sizes of 16, 32, 64, and so on, up to M_{max}. For instance, if the maximum number of available transmit antennas is set to 64, the possible values for M would be 16, 32, and 64. In this work, the optimization process is conducted for three different values of M_{max}, specifically 128, 256, and 512, each offering a distinct set of discrete options for M. These variations allow for evaluating the impact of transmitter array size on system performance and RIS-assisted link efficiency.

To define the transmit power P_{t} utilized by the transmitter, we focus on optimizing $\rho = \frac{P_{\text{t}}}{\sigma^2}$. Various values of ρ have been considered in the literature, such as $\rho = 5$ dB in [9]. In this study, we assume that the minimum transmitter configuration, M_{min}, corresponding to a 16-element antenna block, achieves a baseline of $\rho = 0$ dB. As the algorithm increases the number of transmitter elements to the next block size (e.g., $M = 32$), the available transmit power budget is adjusted to improve ρ, allowing values from 0 dB up to 3 dB. More generally, each doubling of M results in a 3 dB increase. This strategy aligns with the physical interpretation that increasing the array size enhances directional gain, thereby improving ρ. Accordingly, the optimization algorithm evaluates all possible combinations of M and transmit power for each M_{max}, ultimately selecting the configuration that provides the most favorable trade-off between link quality and power consumption.

The next step involves calculating the best beamforming codebook vector, $\mathbf{f}_{\text{BI}}$, used for transmission from the BS to the RIS. These calculations are based on the randomly selected M positions. Additionally, depending on the user location and the value of B, the algorithm calculates $\mathbf{v}$, which represents the best beam used to transmit from the RIS to the blocked user.

The initial value of the number of subcarriers, K, is set to 1 and is incremented cautiously due to the associated computational complexity. To constrain the system complexity and maintain practical feasibility, a threshold is introduced, limiting the maximum number of RIS elements to 1000. This threshold is based on our previous findings in [8], where 1000 elements were required to establish a reliable RIS-assisted link for a PHO. In the present work, the primary objective is to reduce the required number of RIS elements N while achieving comparable performance. Once the algorithm computes N using the current values of system parameters, it compares the result against the defined threshold. If the computed value exceeds the threshold, K is incremented, and the process is repeated to recompute N. This iterative procedure continues until the condition $K \leq K_{\text{max}}$ is satisfied, ensuring that the optimal combination is selected to minimize N without exceeding the maximum permissible complexity.

Algorithm 2 PSO for RIS configuration time.

Choose population size *num_particles*, number of iterations, inertia weight *w*, cognitive coefficient *c1*, and social coefficient *c2*.
Initialize the subcarriers values with $K = 1$ and set the value of K_{max} and B.
Set the threshold value of RIS elements when exceeded K is incremented afterwards.
Set the minimum M_{min} and maximum M_{max} values for *M* with increment of multiples of (block size).
Initialize particle positions *M* as random multiples of the block size within the range $[M_{\text{min}}, M_{\text{max}}]$.
Initialize P_t depending on the selected MIMO block between [*P_min*, *P_max*]
for iter = 1 to *num_iterations* **do**
    for each particle from *num_particles* **do**
        Evaluate Calculate $\mathbf{f}_{\text{BI}}$,$\mathbf{v}$.
        Evaluate *N* and RIS square area.
        if *N* exceeds of threshold RIS elelments. **then**
            Increment *K*
        end if
        if current N value is better than best local value **then**
            Update best local values (N,*M*, P_t,K ,$\mathbf{f}_{\text{BI}}$,$\mathbf{v}$).
        end if
        if current N value is better than global best value **then**
            Update global best values (*M*, P_t,K ,$\mathbf{f}_{\text{BI}}^\star$, $\mathbf{v}^\star$).
        end if
    end for
    for each particle **do**
        Update velocities PSO velocity update equations.
        Update particle positions and ensure values remain within ranges.
        if *K* exceeds K_{max} **then**
            Set *K* to K_{max}.
        end if
    end for
end for
return Optimized N, T_c, Best values : M, $\mathbf{f}_{\text{BI}}^\star$, $\mathbf{v}^\star$, K, P_t.

At this stage, the best personal (local) value of N is updated based on the minimum value across all particles. The global best position is also updated to achieve the minimal N across all iterations, which is then returned as the optimized N. Additionally, the algorithm determines the optimal set of parameters required to achieve the desired R at the optimized N. These include the required transmitter array M, the optimal BS beam $\mathbf{f}_{\text{BI}}^{\star}$ transmitting to the RIS, the optimal RIS beam $\mathbf{v}^{\star}$ transmitting to the user, and the best number of subcarriers allocated for the user.

It is important to note that equations (14) and (20) are derived based on the approximation of a squared array area [31]. Consequently, the optimization process involves determining the optimal N. Since the optimized N may not yield a perfect square area, it is approximated to the nearest square area of then T_c is calculated. Further details about the area approximation are provided in the results section.

C. Computational complexity

The computational complexity associated with minimzing T_c depends on the considered scenario. In the continuous phase shift, the RIS beamforming vector is analytically derived to counteract the angle-of-arrival and angle-of-departure components, eliminating the need for RIS optimal beam search. The complexity in this case primarily arises from evaluating the achievable rate over a finite set of transmit-side beams $\mathcal{F}$, resulting in a complexity on the order of $\mathcal{O}(|\mathcal{F}| \cdot K)$, where K is the number of allocated subcarriers to a blocked user.

In contrast, the discrete phase shift scenario requires joint optimization over quantized RIS beams and transmit beams, typically from codebooks of sizes $|\mathcal{V}|$ and $|\mathcal{F}|$, respectively. The joint beam search thus incurs a complexity of $\mathcal{O}(|\mathcal{V}| \cdot |\mathcal{F}| \cdot K)$, which grows significantly with beam resolution. Therefore, while the continuous case offers lower computational overhead, the discrete case requires exhaustive or heuristic search over a larger beam codebook solution space, making it computationally more demanding.

IV. Suggested RIS-Assisted PHO Framework

In this work, the bus in Fig. 2 prevents ULA sector 1 from establishing a LoS link to the user. When this blockage event is detected by the VAWC framework integrated with the BS, it triggers a PHO to ULA sector 2's RIS-assisted link. The new RIS-assisted link will be selected from a subset of VLoS beam indices stored at the BS as part of the RIS-assisted CKM database (see Fig. 1).

The PSO algorithm determines the optimal M used in ULA sector 2 and the optimal N for the RIS required to establish the link to the blocked area based on the desired rate. Additionally, the RIS-assisted CKM contains the optimal parameters, calculated based on the outcome of the PSO algorithm performed using an offline estimation approach, to enable a fast response during online scenarios. These parameters include the optimal beams $\mathbf{f}_{\text{BI}}^{\star}$, $\mathbf{v}^{\star}$, and the corresponding transmitted power to the blocked location. Finally, the PSO algorithm will determines T_c based on the optimized value of N, and T_c will be incorporated as an additional time to execute the updated PHO timing requirements, as shown in Equation (3), ensuring a smooth and accurate timing to trigger the PHO procedure.

V. Performance Evaluation and Results

The work in this paper adopts the simulation environment described in [8], where the VAWC framework detects blockage events, user locations, and obstacle locations as explained in the next section.

A. Simulation Environment

The simulation environment is based on the colocated camera blockage scenario presented in the dataset [29]. Below are the key notes of the simulation environment:

- The VAWC system monitors a 90×15-meter street, where the length of the street aligns with the x-axis, and the width corresponds to the y-axis. The street is located in the xy plane at $z = 0$, with the point of origin at the upper right corner of the street, as shown in Fig. 2.
- A BS is positioned at $(x = 45)$ at mid point of the 90 street. The BS, set at a height of 5 meters, is equipped with cameras providing a panoramic view of the street. An RIS supports the BS mounted on a building behind it, located at $(45, -5)$ with a height of 6 meters. The blockage is modeled by a bus obstructing the LOS link in certain segments of the street.
- The pre-established CKM enables the RIS to steer the signal to the car shown in Fig. 2. The car lane is represented as a straight-line trajectory at $y = 9$, extending from the point $(0, 9)$ to the point $(90, 9)$.
- Depending on the user's location and movement speed, the VAWC in [6] determines the optimal time to trigger a PHO based on T_W in equation (1). In this work, we propose a new time to trigger the PHO, represented by $T_{\text{W}}^{\text{RIS}}$ as presented in equation (3), which accounts for T_c of the optimized RIS area.

In this simulation, we focused on a section of the street experiencing signal blockage, specifically between $x = 15$ and $x = 22$ meters. The RIS is dedicated to providing coverage for this segment of the street.

B. Simulation Results

The proposed algorithm computes the optimal values of N and T_c. As discussed previously, equations (14), (20), and (25) are derived under the assumption of a squared array area approximation, as outlined in [31]. Accordingly, the optimization process entails identifying the optimal N, which may not always correspond to a perfect square. In such cases, the algorithm approximates the result to the nearest perfect square to facilitate practical deployment. An illustration of this procedure is shown in Fig. 5(a). Under the ideal continuous phase shifter scenario, the optimal number of RIS elements across various locations within the coverage area was found to range from 345 to 350 elements, depending on the user's position. Since these values do not form a perfect square, the algorithm approximates them to $N = 361$ elements, arranged in a 19×19 square grid, to ensure structural compatibility

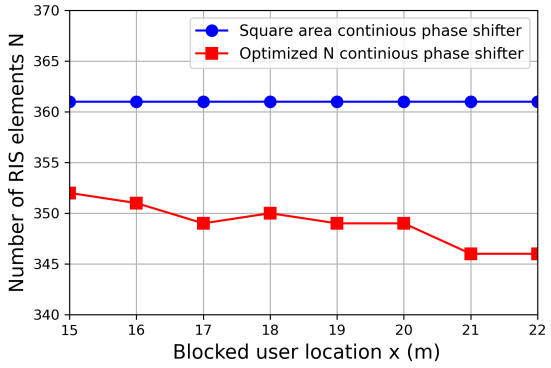

(a) Optimized N and approximated RIS square area, continuous phase shifter scenario.

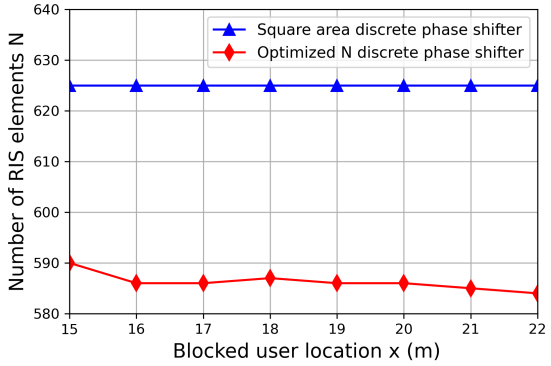

(b) Optimized N and approximated RIS square area, discrete phase shifter scenario $B = 3$.

Figure 5: Comparative plots of RIS square area and Optimized N for both continuous and discrete phase shifter scenarios.

and performance consistency. It is also worth mentioning that when the blocked user is closer to the BS located at $x = 45$, fewer RIS elements are required. This is clearly demonstrated in the optimized N graph, where the user at $x = 15$ requires more RIS elements than the user at $x = 22$, as it is farther from the BS.

In the second scenario, which assumes the use of a discrete phase shifter with a resolution of $B = 3$ bits, the optimal values of N were found to range from 585 to 600. The algorithm then approximates this range to $N = 625$, corresponding to a square grid of 25×25 elements. The results presented in Fig. 5(b) demonstrate that while the ideal continuous phase shifter offers a lower number of required elements and faster computational convergence, it may result in impractical deployment scenarios. Nonetheless, the reduced computational complexity makes this scenario more suitable for real-time or online estimation applications.

The results presented in Fig. 6 illustrate the impact of subcarrier allocation on the required RIS area to achieve a target link rate R. The optimization algorithm identifies two viable configurations: a larger RIS with fewer allocated subcarriers or a smaller RIS supplemented by a greater number of subcarriers. This trade-off is evaluated at various locations along the street, as shown in the figure. For instance, at

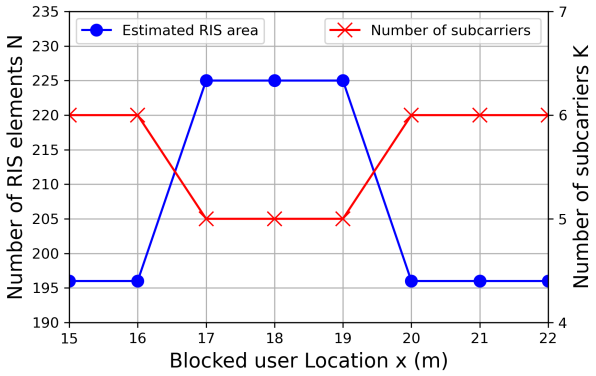

Figure 6: Trade-off between RIS area and number of subcarriers for the same achievable rate $R_{\text{th}} = 1$ (continuous phase shifter scenario).

location $x = 16$, the optimized RIS size is $N = 196$ elements with $K = 6$ subcarriers. Conversely, at location $x = 19$, the algorithm selects a larger RIS with $N = 225$ elements while reducing the subcarriers to $K = 5$. These findings underscore the influence of subcarrier allocation on RIS-assisted link efficiency. Allocating a greater number of subcarriers can compensate for a reduction in RIS size while maintaining the required link performance. This results in faster RIS configuration times and reduced signal processing complexity, owing to the deployment of fewer RIS elements for establishing the VLoS link.

Fig. 7 is consistent with the preceding results, illustrating the required RIS area and the corresponding subcarrier allocation across various segments of the blocked region. Fig. 7(a) depicts the variation in RIS area with respect to different achievable rate targets. The estimated square RIS areas range from $N = 289$ elements, arranged in a 17×17 grid for the lowest achievable rate of $R = 1$, up to $N = 841$ elements, arranged in a 29×29 grid for the highest rate of $R = 6$. Fig. 7(b) presents the associated subcarrier allocations required for each RIS configuration to maintain the same achievable rate. For $R = 1$, the number of allocated subcarriers varies between $K = 11$ and $K = 12$, depending on the RIS area, whereas for $R = 6$, the required number of subcarriers reaches $K = 24$. It is worth mentioning that, the proposed algorithm was able to achieve higher rates with the same RIS area by increasing the allocated subcarriers. This is represented by the overlap of the $R = 2$ and $R = 3$ curves in Fig. 7(a). However, for higher rates, both the RIS area and the allocated subcarriers needed to be increased in order to achieve the desired R.

These findings highlight an important trade-off: the allocation of additional subcarriers can compensate for a reduction in RIS area to achieve a given target rate, and vice versa. This enables the system to flexibly balance between hardware complexity and signal processing load. Consequently, once the RIS area is fixed to meet configuration time constraints, dynamic subcarrier allocation can be employed to acquire the achievable rate based on user demands without requiring physical modifications to the RIS structure.

The results in Fig. 8 highlight another factor that contributes to minimizing the RIS area: the use of narrower beams

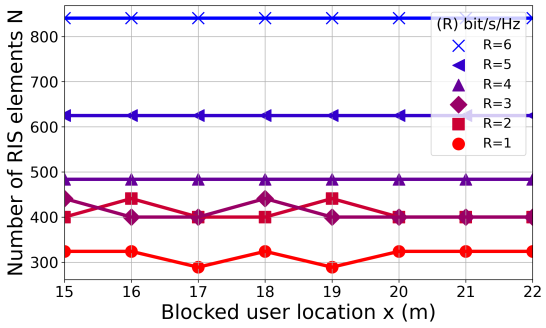

(a) Effect of RIS area on the achievable rate

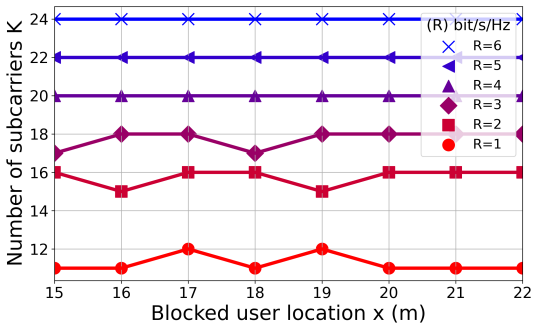

(b) Effect of subcarriers on the achievable rate

Figure 7: Comparative plots of RIS area and subcarrier effects on achievable rates (discrete phase shifter $B = 3$, $M = 512$).

projected onto the RIS by increasing the number of transmitter MIMO elements. This figure illustrates the correlation between the number of subcarriers K, the number of transmitter MIMO elements M, and the required RIS area for different values of R. In general, increasing the number of MIMO elements enhances performance. A comparison of $M = 128$, $M = 256$, and $M = 512$ shows that a transmitter with $M = 512$ requires a smaller RIS area to achieve the same data rate, particularly noticeable at $K = 6$. Another perspective on the impact of the transmitter MIMO can be observed for $R = 1$, where both $M = 512$ and $M = 256$ share the same RIS area. However, the $M = 512$ transmitter requires only four subcarriers to achieve the required link rate, whereas the $M = 256$ transmitter requires five subcarriers. Overall, larger MIMO arrays consistently deliver better performance while reducing the need of other resources, either by reducing the required number of subcarriers or by minimizing the RIS area.

Fig. 9 illustrates the relationship between the RIS configuration time T_c and the performance of the RIS-assisted link, evaluated in terms of the achievable rate R and the required RIS area necessary to attain that performance level. The configuration time is estimated based on a shift register operating at a clocking rate of $C_{lk} = 100\,\text{kHz}$ [10]. Fig. 9(a) presents the performance results for the continuous phase shift scenario under varying target rates. For the lowest achievable rate ($R = 1$), a RIS composed of $N = 225$ elements is sufficient, resulting in a configuration time of approximately

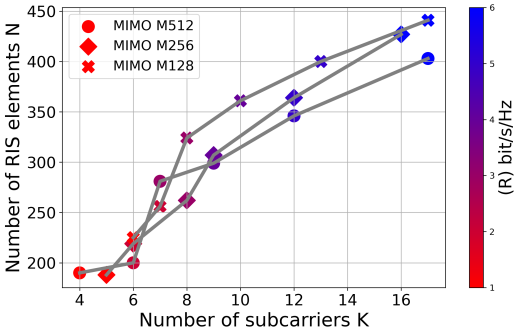

Figure 8: Effect of transmitter MIMO on achievable rate, RIS area, and subcarriers (continuous phase shifter scenario).

$T_c = 2\,\text{ms}$. Conversely, to achieve the highest rate ($R = 6$), the required RIS area increases to $N = 441$ elements, yielding a configuration time of approximately $T_c = 9\,\text{ms}$. These results underscore the importance of minimizing the RIS area to achieve faster configuration responses, which is critical for latency-sensitive applications such as autonomous vehicular communication. Hence, optimizing the RIS configuration to use the smallest feasible number of elements becomes essential in such scenarios.

Similarly, Fig. 9(b) presents the results of the optimization algorithm under the discrete phase shifter scenario with $B = 3$. In this case, achieving the lowest rate ($R = 1$) requires a larger RIS area of $N = 324$ elements compared to the continuous phase shift scenario, resulting in a configuration time of approximately $T_c = 10\,\text{ms}$. To support the highest rate ($R = 6$), the required RIS area increases significantly to $N = 841$ elements, yielding a configuration time of approximately $T_c = 25\,\text{ms}$. These findings indicate that while modeling the RIS under a continuous phase shifter assumption can reduce computational complexity, it considerably underestimates the minimum RIS size required to sustain reliable link performance. Accurately mapping the RIS area and the corresponding configuration time is essential not only for achieving the desired link rate but also for ensuring seamless handover timing, particularly in mobile scenarios. Although the continuous phase assumption may be advantageous for real-time estimation due to its simplicity, relying solely on this approximation in practical deployments may result in connection interruptions and degraded link quality.

Based on the findings presented above, the required RIS area to achieve the highest rate is $N = 841$, corresponding to a configuration time of $T_c = 25\,\text{ms}$. To account for the impact of the RIS configuration time on the PHO framework discussed in [8], the original T_W value estimated in [6] must be updated to $T_{\text{W}}^{\text{RIS}}$, as detailed in equations (2) and (3). For instance, in [6], a scenario is considered where a blocked user, represented by a vehicle, moves towards the blockage area at a speed of 10 miles per hour. The original estimation of $T_W = 4.7\,\text{seconds}$ was provided before triggering handover to a second BS. IN our work, to ensure accurate triggering of the PHO by an RIS-assisted link instead of a second BS, the updated value $T_{\text{W}}^{\text{RIS}}$ must be used, which accounts

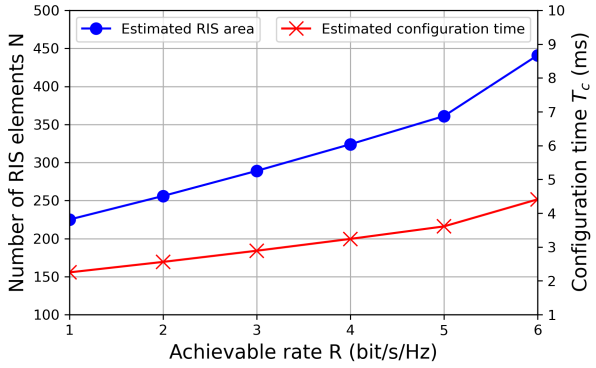

(a) Configuration time of RIS (continous phase shifter).

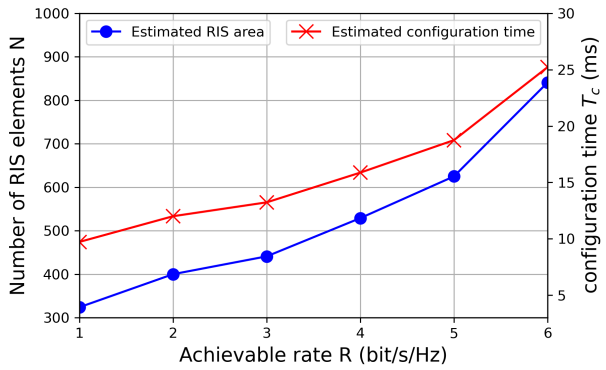

(b) Configuration time of RIS (discrete phase shifter $B = 3$)

Figure 9: Comparative plots of achievable rates effects RIS area and configuration time.

Table II: Updated triggering time for PHO from The Work in [6] with constant car Speed Of 10mph

RIS Area	R (bit/s/Hz)	T_c (ms)	T_W^{RIS} (s)
324	1	9.72	4.69028
400	2	12.00	4.68800
441	3	13.23	4.68677
529	4	15.87	4.68413
625	5	18.75	4.68125
841	6	25.23	4.67477

for the additional timing constraint introduced by the RIS configuration response. In the case of considering an RIS-assisted link established by an RIS with an area of 841 elements, ensuring link performance of $R = 6$, the RIS configuration time is $T_c = 25$ ms, leading to an updated value for $T_{\text{W}}^{\text{RIS}} = 4.67477$ s. This value can be used by the RIS-assisted PHO framework to trigger the handover accurately.

Table II presents the optimal handover triggering time, accounting for the RIS configuration response. The listed RIS areas correspond to different achievable rates. For an RIS area of 841 elements, the PHO algorithm can safely trigger the process with sufficient timing margin, ensuring the RIS-assisted link achieves an achievable rate of $R = 6$. The remaining user movement speeds and their corresponding T_W values from [6] can be updated in a similar manner.

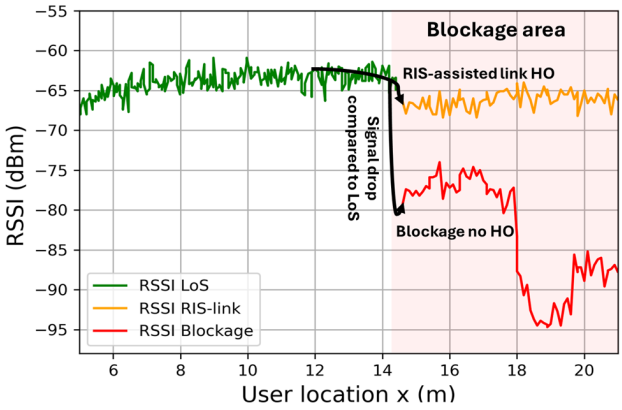

Figure 10: Comparison of RSSI for LoS, RIS-assisted, and Blockage scenarios with and without RIS.

Finally, in our previous work [8], performance analysis was conducted for RIS-assisted links in the context of RIS-assisted PHO. The estimated number of RIS elements required to achieve acceptable link performance during a handover to a blocked user was $N = 1000$, with the received signal strength indicator (RSSI) used as the primary evaluation metric.

The results in Fig. 10 present a comparison between three scenarios: (i) the RSSI of the LoS signal, where no blockage impedes the BS from establishing a direct link to the user; (ii) the RSSI of the RIS-assisted link, where a beam is steered from the RIS to the blocked area using parameters optimized by the proposed PSO algorithm, denoted as the *RSSI RIS-link* curve; and (iii) the RSSI values in a blocked scenario without RIS, denoted as the *RSSI Blockage* curve. While the RIS-assisted link shows reduced signal strength compared to the LoS case, it significantly outperforms the blocked scenario without RIS, improving the RSSI by approximately 15 to 30 dBm, depending on blockage severity and user location. The proposed PSO algorithm reduces the required RIS area from $N = 1000$, based on our findings in [8], to $N = 841$, achieving a 15% reduction in the number of RIS elements required to establish the link. This reduction is attained without compromising performance and while enhancing the RSSI relative to the blocked scenario. Moreover, minimizing the RIS area results in faster configuration response, enabling timely beam steering toward the blocked region. By explicitly calculating and incorporating the RIS configuration time into the handover process, the PHO can be triggered more accurately, ensuring uninterrupted service for blocked users, an essential improvement not addressed in our previous work.

VI. Conclusion

This work presents a novel RIS-assisted VAWC framework capable of providing seamless coverage by restoring blocked LoS links in mmWave networks. It further enhances PHO procedures by minimizing the number of RIS elements to ensure faster RIS configuration response. The proposed approach facilitates accurate PHO-triggered handovers, improving mmWave signal reliability in obstructed scenarios. The

optimization process identifies the optimal system configuration to maximize the achievable rate. The results demonstrate a trade-off between the number of allocated subcarriers and the RIS size required to meet performance targets while also highlighting the influence of the transmitter MIMO array on link quality. Additionally, the proposed PSO algorithm efficiently reduces the number of RIS elements required to establish an RIS-assisted link while preserving the desired achievable rate. Finally, incorporating the RIS configuration time into the analysis enhances handover timing accuracy, thus improving PHO decision-making.

REFERENCES

[1] E. G. Larsson and et al., "Massive MIMO for next-generation wireless systems," *IEEE Commun. Mag.*, vol. 52, no. 2, pp. 186–195, Feb. 2014.

[2] S. Kutty and D. Sen, "Beamforming for millimeter-wave communications: An inclusive survey," *IEEE Commun. Surv. Tutorials*, vol. 18, no. 2, pp. 949–973, 2015, second Quarter.

[3] J. He, H. Wymeersch, and M. Juntti, "Channel estimation for RIS-aided mmWave MIMO systems via atomic norm minimization," *IEEE Trans. Wireless Commun.*, vol. 20, no. 9, pp. 5786–5797, Sep. 2021.

[4] M. Alrabeiah and et al., "Vision aided URLLC communications: Proactive service identification and coexistence," in *Asilomar Conf. Signals, Syst., Comput.* Pacific Grove, CA, USA: IEEE, Nov. 2020, pp. 174–178.

[5] H. Okamoto and et al., "Machine-learning-based throughput estimation using images for mmWave communications," in *2017 IEEE 85th Veh. Tech. Conf. (VTC Spring)*. IEEE, June 2017, pp. 1–6.

[6] M. Al-Quraan and et al., "Intelligent beam blockage prediction for seamless connectivity in vision-aided next-generation wireless networks," *IEEE Trans. Netw. Serv. Manag.*, vol. 20, no. 2, pp. 1937–1948, Jun. 2022.

[7] L. Mohjazi and et al., "An outlook on the interplay of AI and software-defined metasurfaces: An overview of opportunities and limitations," *IEEE Veh. Technol. Mag.*, vol. 15, no. 4, pp. 62–73, Dec. 2020.

[8] A. Adnan and et al., "Performance evaluation of IRS-Assisted Intra-cell handover in vision-aided mmWave networks," in *2024 IEEE Wireless Comm. and Net. Confe. (WCNC)*. Dubai, United Arab Emirates: IEEE, Apr. 2024, pp. 1–6.

[9] S.-K. Chou and et al., "On the aperture efficiency of intelligent reflecting surfaces," *IEEE Wireless Commun. Lett.*, vol. 10, no. 3, pp. 599–603, Mar. 2021.

[10] J.-B. Gros and et al., "A reconfigurable intelligent surface at mmWave based on a binary phase tunable metasurface," *IEEE Open J. Commun. Soc.*, vol. 2, pp. 1055–1064, May 2021.

[11] C. Feng and et al., "Near-field modeling and performance analysis for extremely large-scale IRS communications," *IEEE Trans. Wireless Commun.*, vol. 23, no. 5, pp. 4976–4989, May 2024.

[12] Y. Lu and L. Dai, "Near-field channel estimation in mixed LoS/NLoS environments for extremely large-scale MIMO systems," *IEEE Trans. Commun.*, vol. 71, no. 6, pp. 3694–3707, Jun. 2023.

[13] M. Al-Quraan and et al., "Enhancing reliability in federated mmWave networks: A practical and scalable solution using Radar-Aided dynamic blockage recognition," *IEEE Trans. Mobile Comput.*, vol. 23, no. 10, pp. 10 146–10 160, Oct. 2024.

[14] M. Alrabeiah, A. Hredzak, and A. Alkhateeb, "Millimeter wave base stations with cameras: Vision-aided beam and blockage prediction," in *2020 IEEE 91st Vehic. Tech. Conf. (VTC2020-Spring)*. IEEE, May 2020, pp. 1–5.

[15] H. Okamoto and et al., "Machine-learning-based throughput estimation using images for mmWave communications," in *2017 IEEE 85th Vehicular Technology Conf. (VTC Spring)*, Jun. 2017, pp. 1–6.

[16] S. Ohta and et al., "Point cloud-based proactive link quality prediction for millimeter-wave communications," *IEEE Trans. on Machine Learning in Commun. and Networking*, vol. 1, pp. 258–276, Sept. 2023.

[17] U. Demirhan and A. Alkhateeb, "Radar aided proactive blockage prediction in real-world millimeter wave systems," in *ICC 2022-IEEE Int. Conf. on Commun.* IEEE, May 2022, pp. 4547–4552.

[18] T. Jiang and et al., "Learning to beamform for intelligent reflecting surface with implicit channel estimate," in *GLOBECOM 2020-IEEE Global Commun. Conf.* IEEE, Dec. 2020, pp. 1–6.

[19] C. Jia and et al., "Machine learning empowered beam management for intelligent reflecting surface assisted MmWave networks," *China Commun.*, vol. 17, no. 10, pp. 100–114, Oct. 2020.

[20] C. You, B. Zheng, and R. Zhang, "Fast beam training for IRS-assisted multiuser communications," *IEEE Wireless Commun. Lett.*, vol. 9, no. 11, pp. 1845–1849, Nov. 2020.

[21] D. Ding and et al., "Environment-aware beam selection for IRS-aided communication with channel knowledge map," in *Proc. IEEE Globecom Wkshps (GC Wkshps)*. IEEE, Dec. 2021, pp. 1–6.

[22] G. C. Alexandropoulos and et al., "RIS-enabled smart wireless environments: Deployment scenarios, network architecture, bandwidth and area of influence," *EURASIP J. Wireless Commun. Netw.*, vol. 2023, no. 1, p. 103, Jan. 2023.

[23] M. Rossanese and et al., "Designing, building, and characterizing RF switch-based reconfigurable intelligent surfaces," in *Proc. 16th ACM Workshop Wireless Netw. Testbeds, Exp. Eval. & Char.*, Oct. 2022, pp. 69–76.

[24] X. Pei and et al., "RIS-aided wireless communications: Prototyping, adaptive beamforming, and indoor/outdoor field trials," *IEEE Trans. Commun.*, vol. 69, no. 12, pp. 8627–8640, Dec. 2021.

[25] J. Rains and et al., "High-resolution programmable scattering for wireless coverage enhancement: an indoor field trial campaign," *IEEE Trans. Antennas Propag.*, vol. 71, no. 1, pp. 518–530, Jan. 2022.

[26] Y. Liu and et al., "Reconfigurable intelligent surfaces: Principles and opportunities," *IEEE Commun. Surv. Tut.*, vol. 23, no. 3, pp. 1546–1577, May 2021.

[27] S. Hassouna and et al., "Indoor field trials for ris-aided wireless communications," in *2023 IEEE Int. Symp. Antennas Propag. USNC-URSI Radio Sci. Meet. (USNC-URSI)*. IEEE, Jul. 2023, pp. 75–76.

[28] M. Al-Quraan and et al., "Federated learning for reliable mmwave systems: Vision-aided dynamic blockages prediction," in *2023 IEEE Wireless Commun. Netw. Conf. (WCNC)*. Glasgow, UK: IEEE, Mar. 2023, pp. 1–6.

[29] M. Alrabeiah and et al., "ViWi: A deep learning dataset framework for vision-aided wireless communications," in *Proc. IEEE VTC-Spring*. IEEE, May 2020, pp. 1–5.

[30] E. Björnson and L. Sanguinetti, "Power scaling laws and near-field behaviors of massive MIMO and intelligent reflecting surfaces," *IEEE Open J. Commun. Soc.*, vol. 1, pp. 1306–1324, Sept. 2020.

[31] D. Dardari, "Communicating with large intelligent surfaces: Fundamental limits and models," *IEEE J. Sel. Areas Commun.*, vol. 38, no. 11, pp. 2526–2537, Nov. 2020.

[32] P. Wang and et al., "Fast beam training and alignment for IRS-assisted millimeter wave/terahertz systems," *IEEE Trans. Wireless Commun.*, vol. 21, no. 4, pp. 2710–2724, Apr. 2021.

[33] J. He and et al., "Learning to estimate RIS-aided mmwave channels," *IEEE Wireless Commun. Lett.*, vol. 11, no. 4, pp. 841–845, Apr. 2022.

[34] J. Perruisseau-Carrier and et al., "Contributions to the modeling and design of reconfigurable reflecting cells embedding discrete control elements," *IEEE Trans. Microw. Theory Techn.*, vol. 58, no. 6, pp. 1621–1628, Jun. 2010.

[35] M. Abualhayja'a and et al., "How much power is needed for RIS to beat relays? a sustainability framework," *TechRxiv*, Mar 2025.

[36] J. Rains and et al., "Reflecting metasurface unit cell design with multi-bit azimuthal control," in *Proc. Int. Conf. Microw., Antennas & Circuits (ICMAC)*. Chengdu, China: IEEE, December 2021, pp. 1–4.